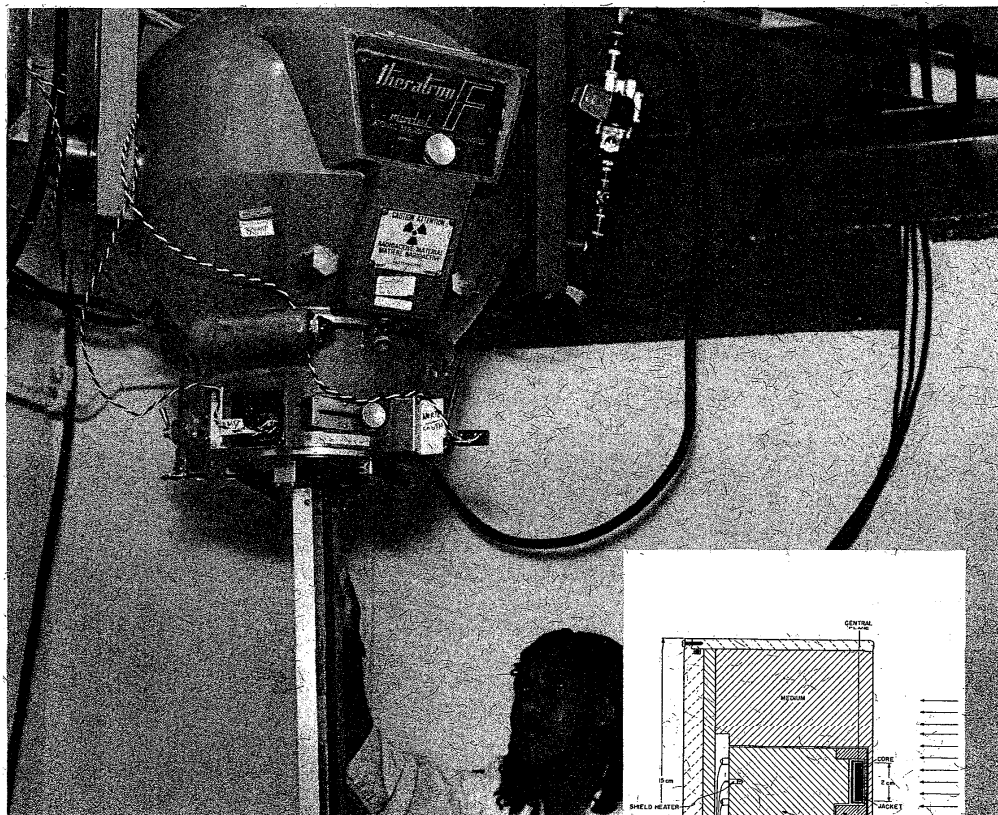
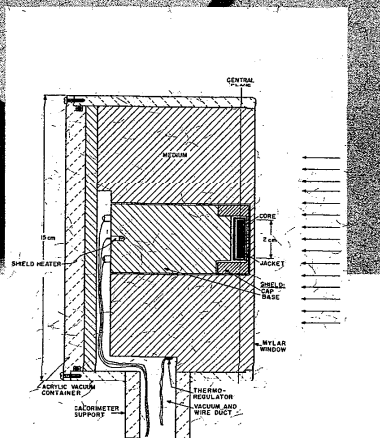


Absorbed-Dose Calibration of Ionization Chambers in a ^{60}Co Gamma-Ray Beam



NIST
Special
Publication
250-40



John S. Pruitt

NIST MEASUREMENT SERVICES:

Absorbed-Dose Calibration of Ionization Chambers in a ^{60}Co Gamma-Ray Beam

John S. Pruitt

Center for Radiation Research
National Measurement Laboratory
National Institute of Standards and Technology
Gaithersburg, MD 20899

October 1990



U.S. DEPARTMENT OF COMMERCE, Robert A. Mosbacher, Secretary
NATIONAL INSTITUTE OF STANDARDS AND TECHNOLOGY
John W. Lyons, Director

National Institute of Standards and Technology Special Publication 250-40
Natl. Inst. Stand. Technol. Spec. Publ. 250-40, 54 pages (Oct. 1990)
CODEN: NSPUE2

U.S. GOVERNMENT PRINTING OFFICE
WASHINGTON: 1990

For sale by the Superintendent of Documents, U.S. Government Printing Office, Washington, DC 20402-9325

Abstract

Measurement Service C.1 from National Institute of Standards and Technology (NIST) publication SP 250 provides calibrations for customer-owned ionization chambers so that they may be used to determine absorbed dose to water in ^{60}Co gamma-ray beams. The calibrations are based on calorimetric measurement of absorbed dose to graphite in a graphite phantom. Transformation of the calibrations to a water phantom is made with a specially-designed graphite ionization chamber, and requires knowledge of photon mass attenuation coefficients and the perturbation of the graphite chamber in the water medium. The determination of these quantities is described in detail, along with the operational techniques normally used to transfer the calibration to customer-owned chambers. Appendix A lists experimental data used to test the photon-fluence scaling theorem. Appendices B, C, and D describe international comparisons of the chamber calibrations, and Appendix E shows a sample calibration report.

TABLE OF CONTENTS

	<u>page</u>
1. The Calibration Service	1
2. The General Approach	1
3. The Graphite Calorimeter	2
4. The Graphite Transfer Ionization Chamber	6
5. The Chamber Calibrations in a Graphite Phantom	11
6. Calibration Transfer to Water	19
6.1 Theory	19
6.2 Evaluation of the Coefficients	21
6.3 The Chamber Currents in Water	24
6.4 The Absorbed Dose Rate in Water	24
7. Operational Procedures	28
7.1 Exposure Techniques for Various Chambers	28
7.2 Current Measurements and Corrections	29
7.3 Quality Assurance Measurements	31
7.4 Chamber MPPK-281	31
8. Calibration Uncertainties	32
Appendix A Test of the Photon Fluence Scaling Theorem	35
Appendix B U.S. - U.S.S.R. Comparison	41
Appendix C U.S. - Canada Comparison	43
Appendix D U.S. - Sweden Comparison	44
Appendix E Sample Calibration Report	45
References	49

1. The Calibration Service

NIST publication SP 250 lists Measurement Service C.1 (X-Ray and Gamma-Ray Measuring Instruments), which includes the calibration of suitable ionization chambers so that they can be used to determine absorbed dose to water in a phantom irradiated with ^{60}Co gamma rays. The calibrations are based on measurements of absorbed dose with a graphite calorimeter. These measurements have been used to calibrate the vertical 10-kCi ^{60}Co source in room B036 in NIST building 245 so that the absorbed dose rate to water is known as a function of water depth and field size at several positions in the beam.

A report entitled "The Graphite Calorimeter as a Standard for Absorbed Dose for Cobalt-60 Gamma Radiation," has been published [1].¹ It contains much of the information presented in this report.

2. The General Approach

The 10-kCi Theratron F ^{60}Co source in room B036 of NIST building 245 has been mounted on the ceiling of that room to produce a vertical gamma-ray beam, as shown schematically in figure 1. The Theratron head contains adjustable jaws for collimation of the beam. In the work discussed here, the beam cross section was always square, of size $s \times s$ at the collimator, or $f \times f$ at the detector.

The absorbed dose rate in a graphite phantom was measured with a graphite calorimeter at a source distance z_g , and a graphite depth x_g with a field size f_g . The absorbed dose rate in a water phantom at a source distance z_w and a water depth x_w with a field size f_w was obtained from this measurement by a transfer technique utilizing current measurements at the calibration points in both phantoms, with a graphite transfer ionization chamber, published photon mass attenuation coefficients, and a measured chamber perturbation correction. The transformation from the graphite dimensions (z_g, x_g, f_g) to the water dimensions (z_w, x_w, f_w) was determined by the requirement that the photon spectra at the two positions should be similar. As shown in section 6.4 this was accomplished with a simple scaling technique where the scaling factor depended only on the relative densities of atomic electrons in the two phantoms.

By this means the Theratron F source was calibrated so that at a fixed distance z_w the absorbed dose rate to water was

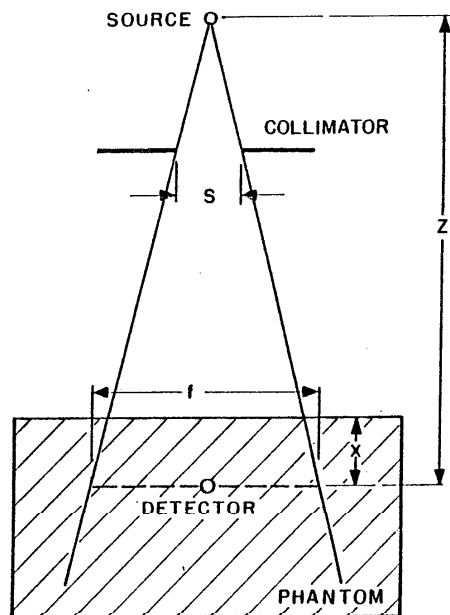


Figure 1. Schematic diagram of vertical ^{60}Co source, showing source distance (z), collimator size (s), field size (f), and phantom depth (x).

¹Numbers in brackets indicate the literature references at the end of the paper.

determined as a function of water depth x_w for several field sizes f_w , in the absence of the chamber. If then another ionization chamber is placed at (z_w, x_w, f_w) , it can be calibrated in terms of the absorbed dose rate to water per unit current, and can be used in other ^{60}Co beams with similar geometry to determine absorbed dose rates.

3. The Graphite Calorimeter

The graphite calorimeter has been described in the NBS Journal of Research in an article entitled "A Heat-Loss-Compensated Calorimeter: Theory, Design, and Performance" [2]. The figures discussed below come from that article.

Figure 2 is a schematic cross section of the calorimeter showing the various elements. The core is a single graphite disc, 20 mm in diameter and 2.75-mm thick. The surrounding jacket consists of a graphite base plate with holes for air evacuation, as shown, and a graphite cap. The jacket dimensions are such that core and jacket have the same heat capacities. The core is mounted on the jacket base plate with polystyrene supports. The jacket is similarly mounted on the much more massive graphite shield and the shield in turn in the even larger graphite medium. All four of these elements, core, jacket, shield, and medium were machined from a single graphite block and have the same density, 1.70 g/cm^3 . Thermal isolation of these four elements is improved by evacuation of the gaps separating them, and by coating the surfaces of the shield and medium with aluminized polyethylene terephthalate, as shown in figures 3 and 4. The shield cap and jacket cap have been removed in figures 3 and 4 to show the core.

Temperature-sensing thermistors are embedded in each of the four components, and the core and shield also each contain a higher resistance thermistor used for heating purposes. The medium is heated by wire coils embedded in its rear surface. Its temperature is maintained at 303 K by the thermoregulator shown in figure 2.

Temperature changes in the various components are measured with the Wheatstone bridge circuit of figure 5, which can be used to follow changes in any of the four temperature-sensing thermistors, C(core), J(jacket), S(shield), and M(medium). Initially, with the calorimeter components at their equilibrium temperatures, the variable resistances are adjusted so that the bridge is balanced in any of the five modes listed in figure 5. R_C (or R_J) equals the resistance of thermistor C (or J), and the currents through thermistors C and J do not change when they are switched out of the bridge circuit. Then the Mode Switch can be moved to any of the five positions without disturbing equilibrium.

The bridge output voltage, between 0 and 0' in figure 5, is amplified and displayed on a chart recorder as a function of time. Figure 6 is a schematic drawing of a typical run, divided into three parts, an initial drift, a heating segment, and a cooling segment. The sawtooth changes during heating are caused by changes in R_x large enough to keep the recorder pen on the chart paper. The temperature rise observed here is proportional to the fractional change in R_x during the run:

$$f_m = \frac{(\Delta R_x + \alpha d_m)}{R_x(0)} \quad (1)$$

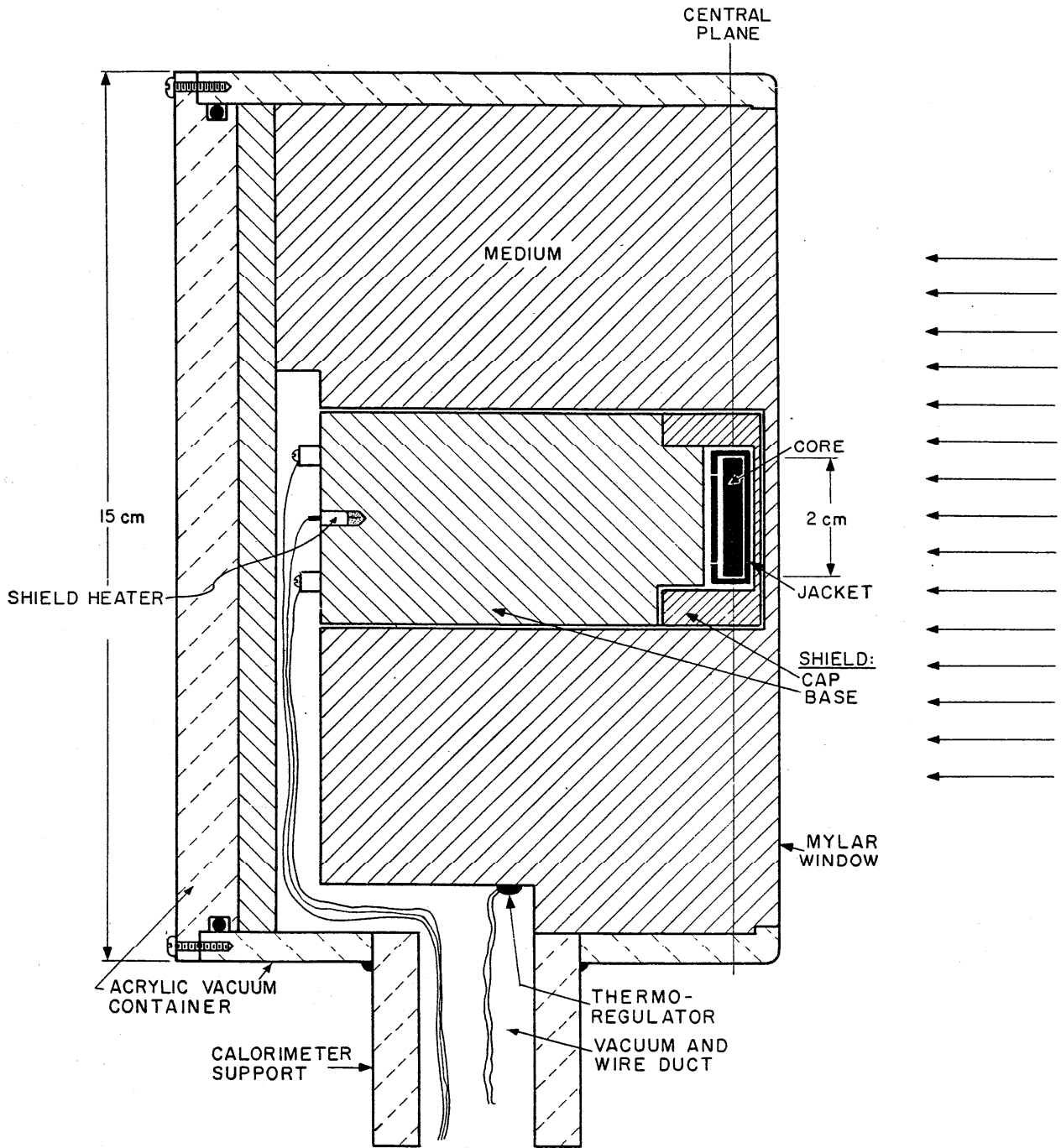


Figure 2. Cross section diagram of graphite calorimeter, showing components core, jacket, shield, and medium.

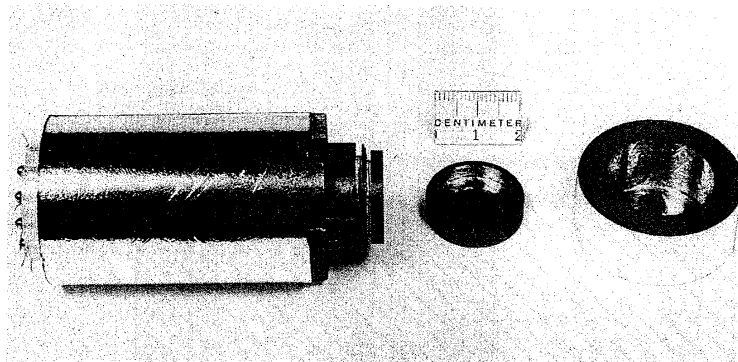


Figure 3. Calorimeter core-jacket-shield assembly with the shield-cap and jacket-cap removed.

where the initial and final values of R_x are $R_x(0)$ and $(R_x(0) - \Delta R_x)$, with $\Delta R_x > 0$, and α is the chart calibration in ohms per scale division. d_m is the chart distance between initial and final drifts, each extrapolated to the mid-run. The total energy is proportional to the observed temperature rise, so:

$$E = k f_m \quad (2)$$

where the constant k is determined from a calibration run.

Chart records for radiation runs and calibration runs look superficially similar, but differ principally because of the size of the correction factors, F , which come from the extrapolations. Returning to figure 6, eq (1) can be rewritten as:

$$f_m = \frac{(\Delta R_x + \alpha d)}{R_x(0)} (1 + F) \quad (3)$$

where d is also shown in figure 6, and:

$$F = \frac{\alpha(d_m - d)}{(\Delta R_x + \alpha d)} \quad (4)$$

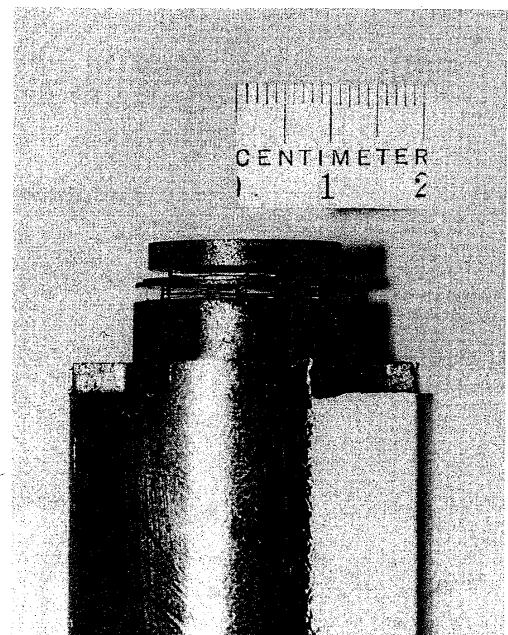


Figure 4. Enlargement of calorimeter core-jacket-shield assembly with the caps removed.

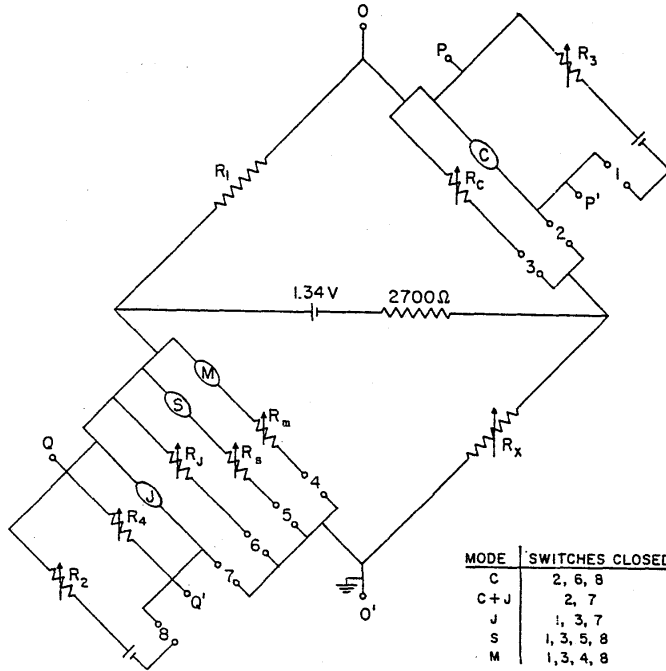


Figure 5. Calorimeter measurement and control circuit, allowing mode changes without changing equilibrium temperatures.

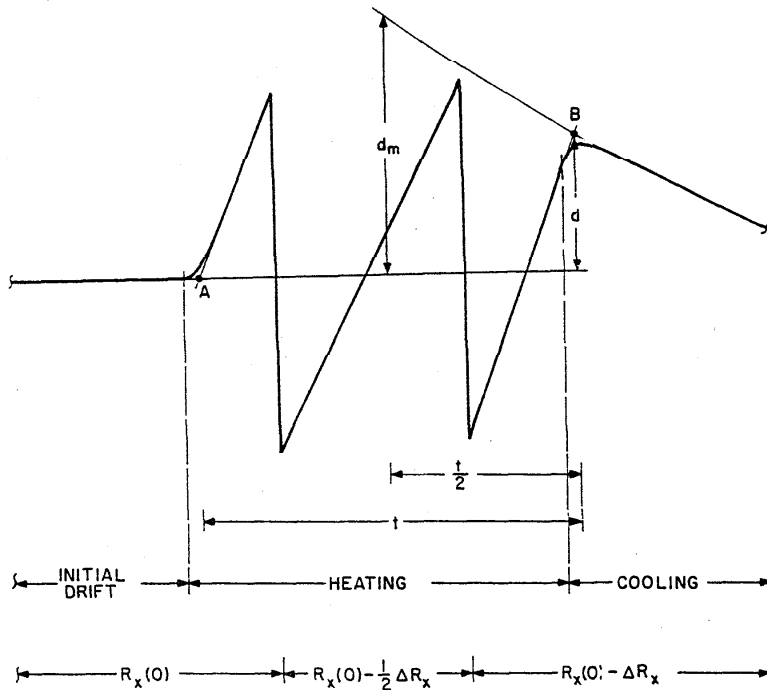


Figure 6. Schematic diagram of a calorimeter chart record, showing the methods used to seek a null and to correct for heat losses.

Correction factors for calibration runs in modes C and C + J, and for radiation runs in mode C are shown as a function of run length in figure 7 as F_C^c , F_{C+J}^c , and F_C^r , respectively. The reason for this behavior is the differences in the heat loss to their surroundings by the calorimeter components contributing to the signal. During radiation runs, core, jacket, and shield are heated uniformly. In mode C only the core contributes to the signal, heat loss to the jacket is negligible except for long runs, and the correction factors are small. During calibration runs the core is heated directly but the jacket and shield are not. The jacket temperature rises slowly because of radiation from the core, but is always much smaller than that of the core. Heat losses from the jacket are much smaller than those from the core, and the correction factors are considerably reduced when the jacket is added to the components contributing to the signal. Thus calibration runs are normally made in the C + J mode and radiation runs in the C mode.

For the calorimeter measurements described in this report, the calorimeter was placed in a ring-shaped graphite phantom, with an inside diameter of 15 cm, an outside diameter of 30 cm, and a depth of 15 cm. This effectively increased the outer diameter of the calorimeter from 15 cm to 30 cm and increased the calorimeter response by as much as 1%, depending on the field size and phantom depth.

4. The Graphite Transfer Ionization Chamber

Figure 8 shows two photographs of a type PL1 ionization chamber, showing the entire chamber and an enlargement of the front end. This chamber was designed for the transfer of calorimetric measurements of absorbed dose from a graphite phantom to a water phantom.² The chamber and its properties were first described in 1976 in a report entitled "Ionization Chamber for Absorbed-Dose Calibration" [3]. Schematic cross sections of the front end and mid-section of the chamber appear in figure 9, showing how the components fit

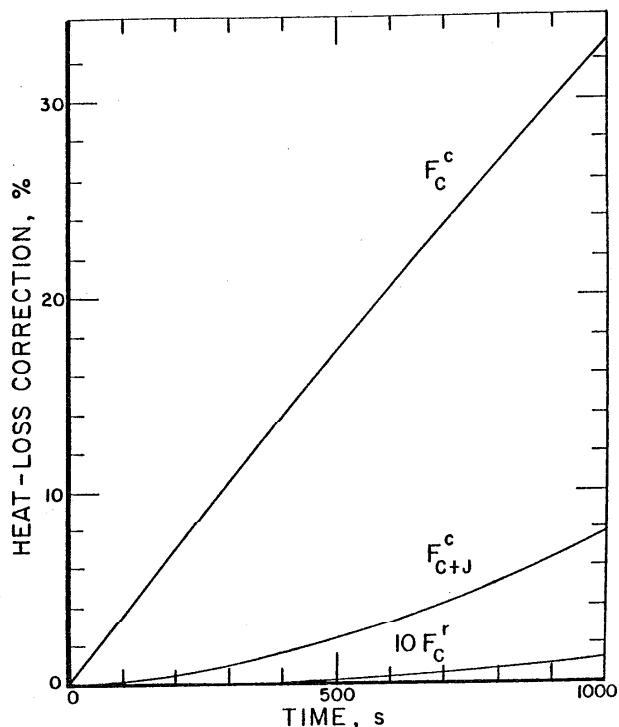


Figure 7. Calculated calorimeter heat loss corrections as a function of time. Subscripts refer to mode, C for core alone, and C+J for core plus jacket. Superscripts refer to type of operation, c for calibration and r for irradiation.

²The chamber shown in figure 8 is PL1-13, made of tissue-equivalent plastic. The other PL1 chambers are graphite, which has less photographic contrast.

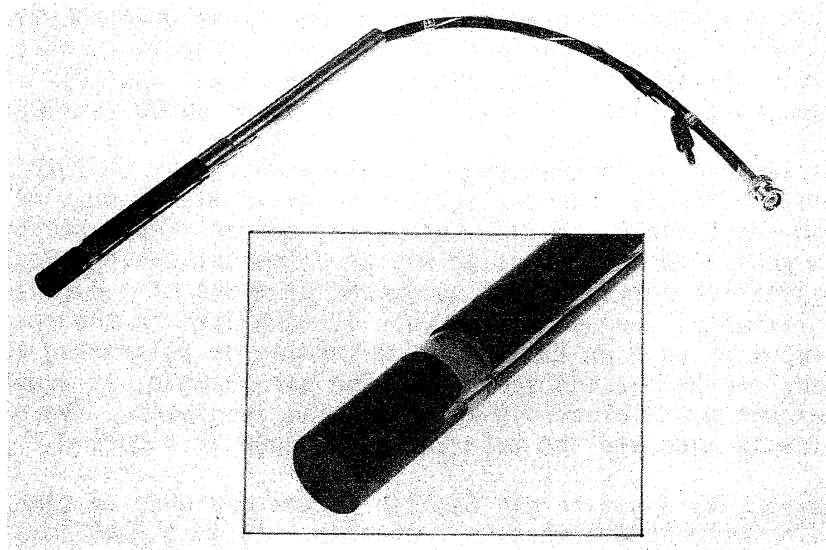


Figure 8. Photographs of PL1-type ionization chamber, showing square-ended high-voltage electrode, high-voltage lead, and air hole.

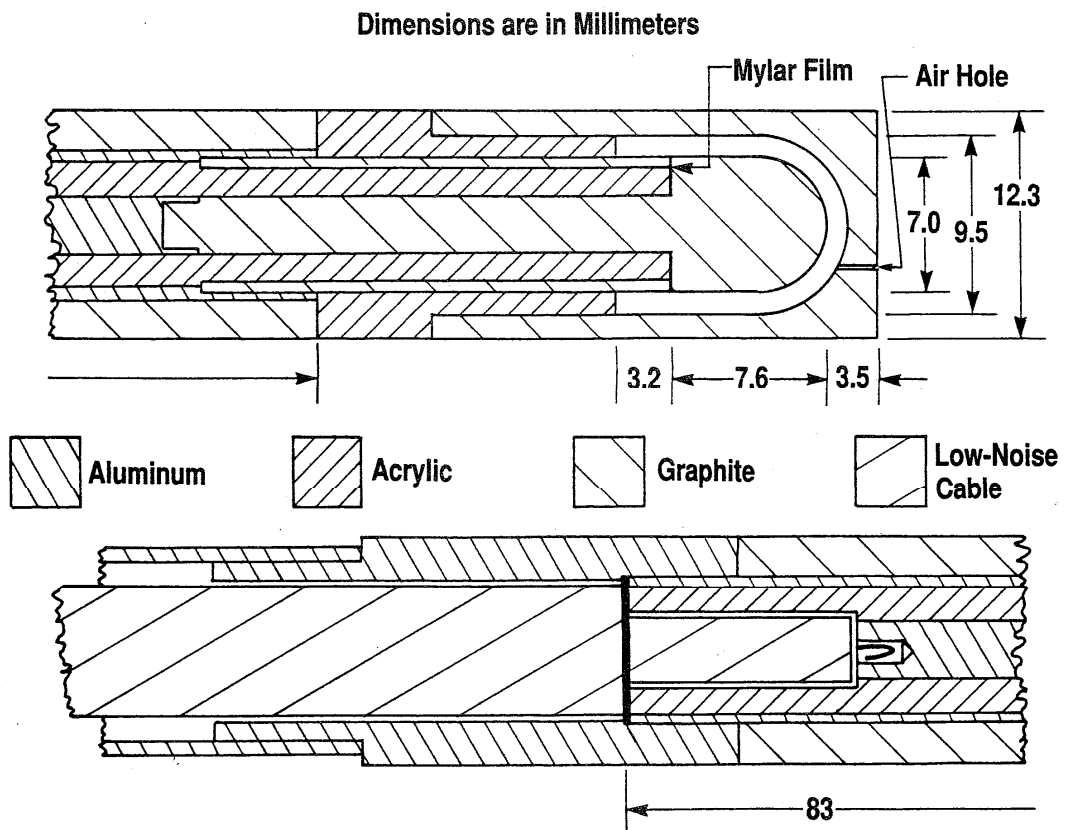


Figure 9. Cross section diagrams of PL1 front end (with air cavity) and middle (with cable connection).

together. They are held together with either clear epoxy or conducting epoxy, depending on whether or not the juncture is meant to transmit current. More detailed dimensions are shown in databook 761, page 19 (DB 761/19). The assembly procedure that proved most useful is described in DB 779/99.

The chamber air gap is thimble shaped, with a thickness of 1.25 mm and an effective volume of 0.3 cm³. The collecting and guard electrodes, on the inside surface of the thimble, are both graphite, and are separated by an 0.08-mm thick polyethylene terephthalate washer. The collecting electrode is connected to the coaxial cable central conductor by means of a 6-cm long aluminum rod. Similarly, the guard electrode is connected to the coaxial cable braid by means of an 8-cm long aluminum tube. The polarizing or high-voltage electrode, on the outside surface of the air thimble, is graphite, and is separated from the guard electrode by an acrylic insulator. The high-voltage connection is made via the separate wire shown in figure 8.

The PL1 chamber has a square end because it was designed to simulate a graphite rod of infinite length when in a phantom. It is placed in a cylindrical hole crossing the phantom and aligned with the center of the air gap, taken to be a point 6.6 mm from the square end, on the beam axis. A passive graphite rod fills the rest of the hole. Since both rod and chamber have square ends, there are no air gaps outside the chamber. The graphite, acrylic plastic, and polystyrene phantoms used for this report are each cylindrical in shape, with the axis of symmetry coinciding with the beam axis. The cylindrical hole in each case runs along a diameter, about 10 mm below the top surface. The water phantom is a plastic box, 30 x 30 cm in cross section, and open at the top. The cylindrical hole in this case is the inside of a plastic tube (12.7-mm I.D., 15.9-mm O.D.) running between the centers of two opposite sides.

There are at present 11 PL1-type chambers available for use, with serial numbers ranging from PL1-10 to PL1-20. The first three, PL1-10 to PL1-12, were constructed in 1974 October. The remaining eight were assembled about 3 years later. Of these, PL1-13 is constructed of A-150 tissue-equivalent plastic, and the other seven are of graphite.

The recombination characteristics of the PL1 chamber are shown in figure 10, which is reprinted from reference [3]. For polarizing potentials less than 60 V, the chamber

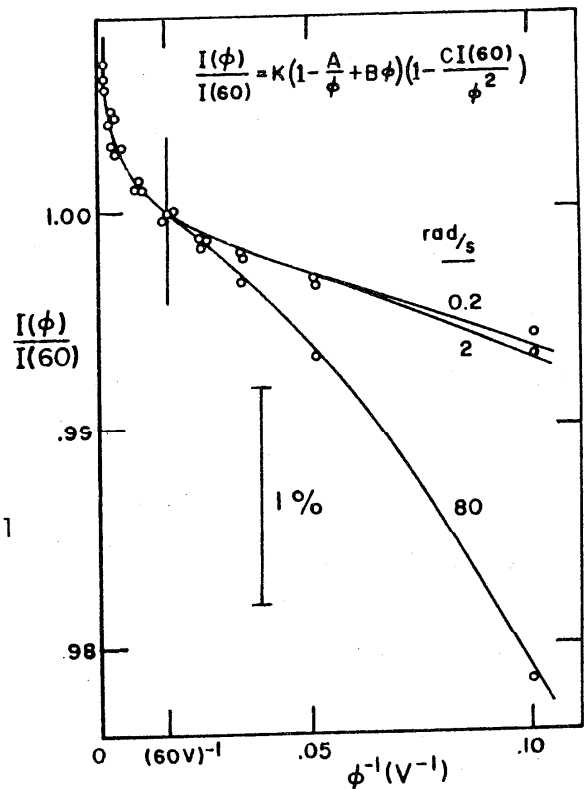


Figure 10. Ion recombination characteristics of PL1-type chamber, showing dependence of ion current on absorbed-dose rate for potentials less than 60 V.

current is a function of the dose rate. For potentials larger than 60 V, ion multiplication appears. At 60 V, the chamber is well behaved and reproducible. Consequently, the PL1 chambers are always used with a polarizing potential of ± 60 V.

The sensitivities of the chambers relative to PL1-11 have been measured on several occasions, in both graphite and water phantoms. These comparisons are summarized in table 1, which comes from DB 827/152. The relative sensitivities range from 1.05 for PL1-10 and PL1-12 to 1.18 for PL1-13. Only PL1-13 shows a large difference in relative sensitivity between water and graphite phantoms (0.75%). Presumably this is because tissue-equivalent plastic does not respond to spectral changes in the same way that graphite does. The original set, PL1-10 to PL1-12 have lower sensitivities because the external sleeves between front and mid-sections (see fig. 9) are made of acrylic plastic rather than graphite.

Table 1. Chamber sensitivities relative to chamber PL1-11. G and W signify graphite and water phantoms, respectively. The coefficient of variation, V, is also shown.

Chamber	Date and Phantom									Average	V, %
	75 Apr G	77 Sep W	77 Dec G	78 Jan G	78 Apr W	79 Mar G	80 Jul G	80 Jul W	81 Jul W		
PL1-10	1.0545	1.0574	1.0540	1.0535	1.0556	1.0547				1.0550	0.13
12	1.0548	1.0557	1.0540	1.0543	1.0548	1.0542				1.0546	0.06
13					1.1848	1.1760				1.1804	0.53
14					1.1219				1.1207	1.1213	0.08
15					1.1011	1.0989				1.1000	0.14
16					1.1244				1.1241	1.1243	0.02
17					1.0918	1.0909	1.0928	1.0911		1.0917	0.08
18					1.0764				1.0756	1.0760	0.05
19					1.1021	1.0995	1.1003	1.0999		1.1005	0.10
20					1.1152	1.1120	1.1133	1.1126		1.1133	0.12

The resistance between collecting and guard electrodes has been measured and recorded for each chamber at several times between 1977 October and 1988 June. The measurement circuit is shown in figure 11, where the source of power was a 1.35 V mercury cell for all except the most recent set of measurements. For the 1988 June set, the source of power was a 1.5 V alkaline cell. As shown in figure 12, the resistances are all between $10^{11} \Omega$ and $10^{15} \Omega$. The original set, PL1-10 to PL1-12 have consistently higher resistances than the more recent models, but they seem to vary by as much as a decade during those 10.7 years.

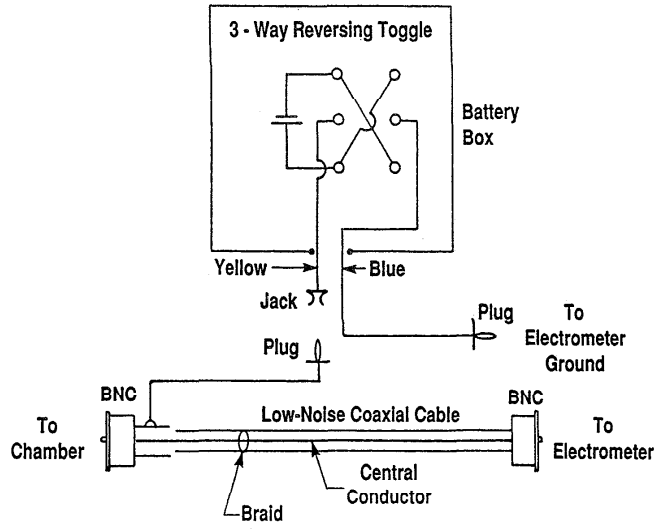


Figure 11. Circuit used to measure input resistances of PL1-type ionization chambers.

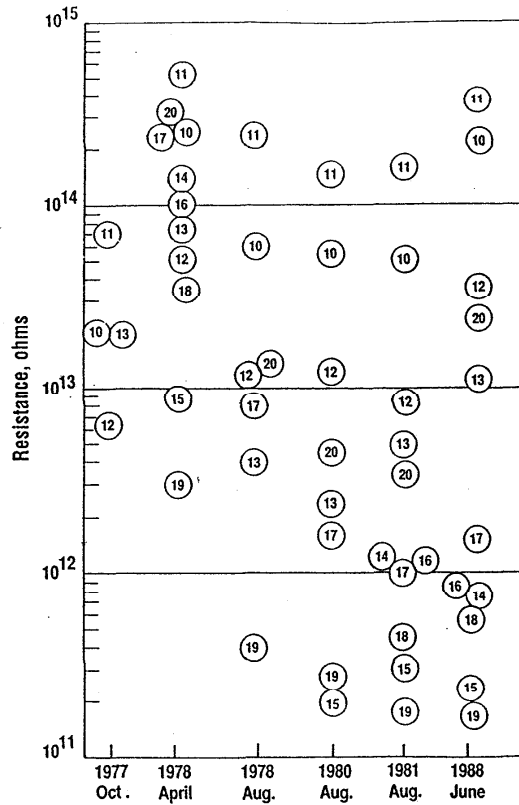


Figure 12. Resistance history of ionization chambers PL1-10 to PL1-20, covering more than 10 years.

All reported PL1 currents in this document are averages of currents measured with positive and negative high voltage polarities. Each measured current is the sum of two components, an ion current generated in the chamber air gap by interaction between air molecules and secondary electrons, and a parasitic current generated in the body of the collecting electrode by secondaries coming to rest. These two components can be separated by making measurements with both positive and negative high-voltage polarity. The ion current component will change sign when the polarity changes, while the parasitic component will not.

If I^+ and I^- are currents measured with positive and negative polarity, respectively, the ion current is:

$$I = \frac{I^+ - I^-}{2} \quad (5)$$

where I^- is normally a negative number. The parasitic current is $(I^+ + I^-)/2$ and may be either positive or negative. It has no immediate application, but is usually recorded because abrupt changes may indicate measurement problems.

The currents reported for customer ionization chambers, on the other hand, are usually measured with a single high voltage polarity, as specified by the customer.

5. The Chamber Calibrations in a Graphite Phantom

The NIST 10-kCi Theratron F ^{60}Co gamma-ray source was calibrated with a graphite phantom at source distances of $z_g = 0.654, 0.80, 0.90, 1.00, 1.10, 1.20,$ and 1.25 m. The beam sizes were determined by square metal jigs temporarily fitted into the collimator opening, with sides of $s = 24.0, 28.0, 33.4, 40.5,$ and 50.8 mm. Not all collimator sizes were used at each distance. The combinations actually used are shown in table 2, which lists the field sizes f_g at the detector. These were calculated from measurements of the beam

Table 2. Field sizes in graphite, f_g , mm

Source distance $z, \text{ m}$	Collimator size $s, \text{ mm}$				
	24.0	28.0	33.4	40.5	50.8
0.654		52	62	75	95
0.800			76		
0.900			86		
1.000		80	95	115	145
1.100			105		
1.200			114		
1.250	86	100	119	144	181

profile at $z_g = 1.00$ m when $s = 33.4$ mm. The profile measurements are shown in figure 13. They were made in air with chamber PL1-11, and its accompanying graphite backup rod, mounted in the water phantom box. What is plotted in figure 13 is chamber current as the box is moved in either a North-South direction or an East-West direction. The box was always positioned so that the direction of motion was perpendicular to the direction of the chamber axis of symmetry. The beam profile does not drop to zero at large distances because of scatter from the bottom of the box, but if this background component is subtracted from the measured currents, and if the field size is defined as the full width at half maximum, the average field size in the two perpendicular directions is 95.2 mm. Since the field size varies as the product of collimator size and source distance, the general equation is:

$$f_g = 2.85 s z_g \quad (6)$$

where f_g and s are in millimeters and z_g is in meters.

The chamber calibrations in graphite were made with the PL1-11 ion chamber in a phantom 30 cm in diameter and 17-cm thick. The NIST portable graphite calorimeter (15 cm in diameter and 10-cm thick) was encased in a graphite sleeve with an inner diameter of 15 cm and an outer diameter of 30 cm. Extra graphite plates were added to the bottom of the calorimeter so that the thickness of graphite behind the calorimeter core was 28 g/cm². In order to protect the calorimeter, it was used with about 2.1 cm of the sleeve phantom projecting above the surface of the calorimeter. It was necessary to correct for scatter from this projecting ring, as discussed below, correcting to a situation where the calorimeter phantom has a flat surface like that of the ion chamber phantom.

The two phantoms were mounted on a sliding table so that they could be alternately inserted into the ⁶⁰Co beam. When in the beam, the center of the calorimeter core and the center of the ion chamber were equidistant from the source. Measurements were made as a function of depth in the phantoms by adding 15-cm diameter graphite discs, surrounded by 30-cm diameter graphite rings (where needed) with a 15-cm internal diameter. The top surface of the discs was seldom in the same plane as the top surface of the rings, but the plane separation was never as large as 3 mm. It was shown in a subsidiary experiment that the error introduced by this mismatch was never as large as 0.1%.

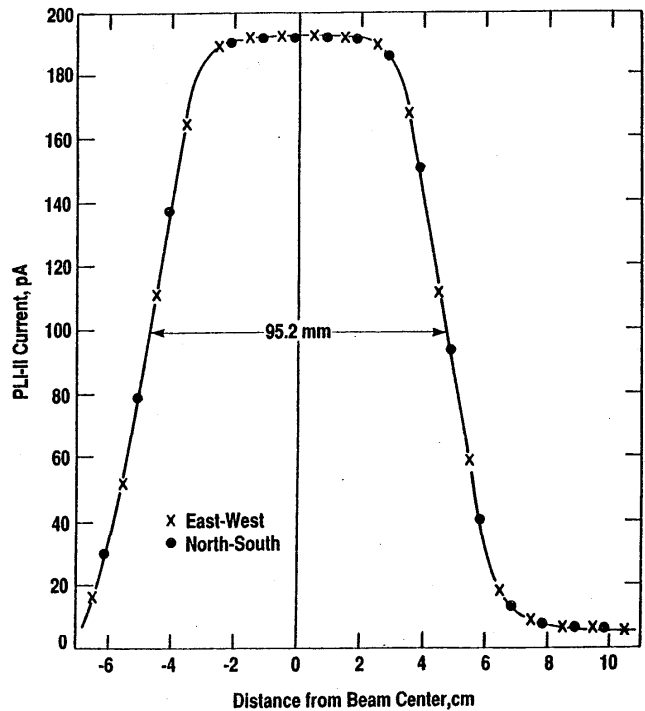


Figure 13. ⁶⁰Co beam profile measured with PL1-type ionization chamber mounted in empty water-phantom box.

The depths in the two phantoms were also never identical but they differed by only 0.03 g/cm². The minimum depth in the ion chamber phantom was 1.62 g/cm², while that in the calorimeter phantom was 0.864 g/cm² for the calorimeter itself plus 0.123 and 0.660 g/cm² for two discs which were always in place, giving a total of 1.647 \approx 1.65 g/cm².

The chamber calibration data are listed in table 3. They were obtained in a series of three experiments performed between August 1978 and April 1979. The earliest experiment was performed at a source distance of $z_g = 1.00$ m (see fig. 1). An initial test of variation with source distance was included, using a single phantom depth (5.08 g/cm²), a single collimator opening (33.4 mm), and source distances of $z_g = 0.8, 0.9, 1.0, 1.1,$ and 1.2 m.³ The second experiment was performed at a source distance of $z_g = 0.654$ m and was immediately followed by measurements at a source distance of $z_g = 1.25$ m. The 0.654 m distance was chosen because as shown in the following section, photon spectra at that distance in graphite are similar to photon spectra at the reference distance of 1.00 m in water. The 1.25-m distance was chosen to provide calibrations suitable for the Soviet intercomparisons described in Appendix B.

The calorimeter data from these experiments are recorded in a file folder labeled "⁶⁰Co measurements in B036" in the possession of Steve R. Domen. Summaries are also included, and copies of these summaries have been inserted in DB 843/44-46. The calorimeter dose rates listed in table 3 are averages of 5 individual runs at $z_g = 0.654$ m and of 10 individual runs at $z_g = 1.00$ m and $z_g = 1.25$ m. The listed dose rates have been corrected for:

- (a) excess scatter from the projecting lip of the ring phantom, mentioned above. These corrections were determined in a subsidiary ion chamber experiment by adding rings to the ion chamber phantom. The results are listed in table 4, which shows that the correction is less than 0.1% if the projecting rings are not directly irradiated, that is, if $f\sqrt{2} < 150$ mm, where f is one side of the square field at the chamber (fig. 1).
- (b) source decay from a reference date ($t = 0$ on 1979 Jan 1, where t is time). The correction factor used was $\exp(0.0003600 t)$, with t measured in days. The coefficient $0.0003600 \text{ day}^{-1}$ was determined from the published ⁶⁰Co half life of 5.2714 years [4].
- (c) shutter timer errors. These were measured with the ion chamber, comparing currents measured with the run length determined by the shutter timer with currents measured with the run length determined by an electronic gate. The shutter timer was found to be in error by 0.078 s, which was added to the original exposure time for each calorimeter run. The runs themselves varied in length from 118 to 365 s, with most about 250 s long.

³The depth 5.08 g/cm² was chosen because it could be reached with both the calorimeter (0.864 + 4.218 g/cm²) and the ion chamber (1.62 + 0.123 + 0.152 + 0.660 + 0.992 + 1.534 g/cm²).

Table 3. Corrected currents and absorbed dose rates in graphite with calibration factors for chamber PL1-11 on 1979 Jan 1 at 22°C and 1 atm.

Source Distance z g m	Graphite Depth P X g g/cm ²	Collimator size, mm														
		s = 24.0			28.0			33.4			40.5			50.8		
		I nA	D mGy/s	N _{graph} Gy/μC	I nA	D mGy/s	N _{graph} Gy/μC	I nA	D mGy/s	N _{graph} Gy/μC	I nA	D mGy/s	N _{graph} Gy/μC	I nA	D mGy/s	N _{graph} Gy/μC
0.654	1.65			0.4581	46.51	101.5	0.4672	47.48	101.6	0.4769	48.50	101.7	0.4894	49.82	101.8	
	3.18			0.4384	44.35	101.2	0.4485	45.45	101.3	0.4596	46.63	101.5	0.4730	48.09	101.7	
	5.84			0.3972	39.95	100.6	0.4095	41.32	100.9	0.4212	42.63	101.2	0.4364	44.28	101.5	
	8.37			0.3534	35.59	100.7	0.3667	36.99	100.9	0.3807	38.45	101.0	0.3979	40.28	101.2	
	11.42			0.3065	30.79	100.5	0.3181	32.09	100.9	0.3334	33.63	100.9	0.3522	35.62	101.1	
	11.59															
0.800 0.900	5.08						0.2824	28.60	101.3							
							0.2239	22.71	101.4							
1.000	1.65			0.1941	19.74	101.7	0.1988	20.27	102.0	0.2032	20.73	102.0	0.2081	21.24	102.1	
	3.18			0.1872	19.00	101.5	0.1922	19.52	101.6	0.1969	20.08	102.0	0.2025	20.61	101.8	
	4.06						0.1819	18.45	101.4	0.1871	19.04	101.8				
	5.08						0.1778	18.01	101.3	0.1826	18.56	101.7	0.1887	19.20	101.7	
	5.84						0.1774	18.00	101.5	0.1826	18.56	101.7	0.1887	19.20	101.7	
	8.37						0.1557	15.73	101.0	0.1616	16.38	101.3	0.1673	17.03	101.7	
1.100 1.200	11.59			0.1367	13.81	101.0	0.1428	14.50	101.5	0.1491	15.16	101.7	0.1564	15.94	101.9	
	5.08						0.1510	15.33	101.5							
1.250	1.65			0.1243	12.70	102.2	0.1273	12.93	101.6	0.1303	13.32	102.2	0.1336	13.62	101.9	
	3.18			0.1203	12.22	101.6	0.1235	12.54	101.6	0.1266	12.92	102.0	0.1303	13.27	101.9	
	5.84			0.1112	11.26	101.3	0.1148	11.64	101.3	0.1184	12.01	101.5	0.1225	12.47	101.8	
	6.38			0.1093	11.10	101.5	0.1148	11.64	101.3	0.1184	12.01	101.5	0.1225	12.47	101.8	
	8.37			0.1012	10.24	101.2	0.1051	10.66	101.4	0.1087	11.07	101.8	0.1135	11.59	102.1	
	11.42			0.0900	9.11	101.3	0.0940	9.54	101.5	0.0981	9.97	101.6	0.1029	10.52	102.3	

Table 4. Measured ring factors, the ratio (PL1-11 current with rings present)/(PL1-11 current with rings removed). The listed σ are standard deviations of the mean of 12 or more measurements. The rings project above the central face of the graphite phantom by (3.05 - 0.59 x) cm.

Source distance z, m	Aperture size s, mm	Phantom depth x, g/cm ²	Ring factor -	σ -
0.654	50.8	1.62	1.0003	0.0000
		3.15	1.0002	0.0001
	40.5	1.62	1.0001	0.0001
		3.15	1.0001	0.0001
1.00	50.8	1.62	1.0023	0.0003
		3.15	1.0016	0.0002
	40.5	1.62	1.0010	0.0002
		3.15	1.0002	0.0005
	33.4	1.62	1.0004	0.0001
		3.15	1.0002	0.0001
	28.0	1.62	1.0007	0.0003
		3.15	1.0003	0.0001
1.25	50.8	1.62	1.0062	0.0003
		3.15	1.0030	0.0001
	40.5	1.62	1.0028	0.0003
		3.15	1.0015	0.0002
	33.4	1.62	1.0015	0.0001
		3.15	1.0007	0.0001
	28.0	1.62	1.0005	0.0001
		3.15	1.0003	0.0001

- (d) impurities in the calorimeter core, using a correction factor of 1.0002 [5].
- (e) The presence of an acrylic plastic ring in the graphite phantom. This ring constitutes the outer wall of the calorimeter, as shown in figure 2, and has an inner diameter of 14 cm and an outer diameter of 15 cm. The correction factor used was 1.0002 [5].

- (f) the presence of an air gap in the calorimeter phantom during the first experiment, where $z_g = 1.00$ m. This gap was produced by plastic tape around the edge of the top surface of the calorimeter, inserted to protect the calorimeter core from excess pressure when extra plates are added. The correction was studied with ion chamber measurements, and the correction factor varied from 1.0001 at $\rho x_g = 3.18$ g/cm² to 1.0005 at $\rho x_g = 11.59$ g/cm², where x_g is depth in the graphite phantom in cm, and ρ is the graphite density in g/cm³.
- (g) radiation escaping from the sides of the phantom. This was studied with ion chamber measurements in a graphite phantom 17.5-cm thick with a diameter which could be changed from 15 cm to 20 cm to 30 cm. The chamber depth could be changed by adding graphite discs on top of the phantom, which at all times had a flat top surface, with no projecting rings. Measurements were made with four different square fields, from 83 x 83 mm to 174 x 174 mm, at a variety of mass depths between 1.4 g/cm² and 39.1 g/cm², using phantom diameters of 15, 20, and 30 cm. The results are listed in internal report NBSIR 77-1203 (September 1978). At each depth for each field size, the measured currents were fitted to a polynomial of the form ($b_0 + b_2 D_p^{-4} + b_4 D_p^{-8}$), where D_p is phantom diameter. From each polynomial could be calculated the percent increase in detector response when D_p is increased from 30 cm to infinity. This is also the percent loss of scattered radiation at that mass depth for that field size. The numbers obtained form a relatively regular array listed as $Y_\beta(\%)$ in table 5 of the internal report. This array was in turn fitted to the equation $Y_\beta(\%) = A \exp(\alpha f_g)$ where f_g is field size in millimeters, and A and α are functions of mass depth, ρx_g , in g/cm²:

$$A = -0.0007 + 0.00113 (\rho x_g)$$

$$\alpha = 0.0277 - 0.00166 (\rho x_g) + 0.000064 (\rho x_g)^2 .$$

(These approximations are valid only for $\rho x_g \leq 14.0$ g/cm².) The correction factor used for radiation escaping from the photon sides is $1 + 0.01 A \exp(\alpha f_g)$, which never exceeded 1.003.

- (h) the presence of vacuum gaps surrounding the calorimeter core and jacket. These gaps perturb the distribution of scattered radiation incident on the core. Monte Carlo calculations of this effect have recently been reported [6] for the NIST calorimeter geometry. These indicate that at mass depths of 5 g/cm² and 17 g/cm², measurements of absorbed dose should be multiplied by correction factors of 1.0020 ± 0.0005 and 1.0050 ± 0.0005 , respectively. The dose rates listed in table 3 have all been multiplied by the factor $(1.00075 + 0.00025 (\rho x_g))$, which reduces to the given factors at 5 and 17 g/cm².

The values of \bar{D} listed in table 3 differ slightly from those in the calorimeter summary (DB 843/44-46) because corrections (g) and (h) had not been applied, and because a decay rate of 0.0003625 day⁻¹ had been used rather than the present rate of 0.0003600 day⁻¹. The values of \bar{D} listed in the ion chamber summaries (DB 810/21-11 and DB 812/32-35) also lack corrections (g) and (h) and in addition had been multiplied by z_g^2 .

The ion chamber data from these experiments are recorded in DB 801/116-200, DB 810/1-14, 137-200, and DB 812/1-30. The results are summarized in DB 812/32-35 for source distances $z_g = 0.654$ m and 1.25 m. The ion chamber currents listed in table 3 have been corrected for:

- (aa) air density changes inside the chamber, using the correction factor $[101.325(T + 273.15)]/[(T_r + 273.15)P]$, where T is air temperature in degrees Celsius, T_r is a reference temperature (22 °C) and P is air pressure in kilopascals (101.325 kPa = 1013.25 mbar = 760 mmHg = one standard atmosphere).
- (bb) source decay from a reference date (t = 0 on 1979 Jan 1, where t is time in days). The correction factor used was $\exp(0.0003600 t)$.
- (cc) telethermometer errors, using a correction factor of 1.0004 (DB 801/148-149).
- (dd) instrumental errors, using a correction factor of 1.0015 (DB 801/7).
- (ee) radiation escaping from the sides of the phantom, using the calorimeter correction (g), above.
- (ff) the difference in mass depth between ion chamber and calorimeter measurements using the same discs. Linear corrections were used, fitted to the two nearest mass depths. For example, for $z_g = 0.654$ m and $s = 50.8$ mm, the partially corrected ((aa) through (ee)) currents at mass depths of 5.84, 8.34, and 11.56 g/cm² in the ion chamber phantom are 0.4369, 0.3983, and 0.3526 nA, respectively. The interpolated currents at the calorimeter mass depths of 5.87, 8.37, and 11.59 g/cm² are 0.4364, 0.3979, and 0.3522 nA, respectively, as shown in table 3. The only mass depth for which this correction was not needed was 5.08 g/cm², which could be attained with different sets of discs for the ion chamber and for the calorimeter, as mentioned earlier.

The currents listed in table 3 do not agree with those in the databook summaries (DB 810/21-22 and DB 812/32-35) because correction (ee) had not been applied to the databook currents, which had been multiplied by z_g^2 , and had used a reference temperature $T_r = 20$ °C in correction (aa) rather than the 22 °C used here.

The graphite chamber calibration factors listed under N_{graph} in table 3 are the simple ratios of dose rate to current. It can be seen that these factors vary with both field size and phantom depth. As shown in reference [1], the graphite calibrations with the 10-kCi Theratron F ⁶⁰Co source can be fitted to the equation:

$$N_{\text{graph}} = N_{\text{graph}}^{\text{ref}} [1 + k_x(1 - \exp[-\gamma_x(\rho x_g - \rho x_g^{\text{ref}})])] + k_f(1 - \exp[-\gamma_f(f_g - f_g^{\text{ref}})])] \quad (7)$$

where $N_{\text{graph}}^{\text{ref}}$ is the value of N_{graph} at the reference mass depth ρx_g^{ref} and the reference field size f_g^{ref} . The exponent coefficients were chosen to be $\gamma_x = 0.25$ cm²/g and $\gamma_f = 0.025$ mm⁻¹. With these choices, the best-fit values

of $N_{\text{graph}}^{\text{ref}}$, k_x , and k_f are listed in table 5, along with ρx_g^r , f_g^r , and the coefficient of variation of each fit.

Table 5. Parameters and coefficients for eq (7), the calibration of chamber PL1-11 in a graphite phantom at 22 °C and 1 atm. The coefficient of variation, V, was calculated for 3 degrees of freedom.

Source distance z_g m	Pre-selected				Least Squares			
	γ_x cm ² /g	γ_f mm ⁻¹	ρx_g^r g/cm ²	f_g^r mm	$N_{\text{graph}}^{\text{ref}}$ Gy/μC	k_x	k_f	V %
0.654	0.25	0.025	5.56	65.4	101.07	-0.00333	0.00595	0.09
1.00	0.25	0.025	5.00	100.0	101.59	-0.00227	0.00465	0.14
1.25	0.25	0.025	5.00	100.0	101.52	-0.00217	0.00411	0.22

The values of $\rho x_g^r = 5.56 \text{ g/cm}^2$ and $f_g^r = 65.4 \text{ mm}$ for the source distance $z_g = 0.654 \text{ m}$ were chosen to transform into the water phantom values $\rho x_w^r = 5.00 \text{ g/cm}^2$ and $f_w^r = 100 \text{ mm}$ at a source distance of $z_w = 1.00 \text{ m}$, as discussed in section 6.4. The transformation of f and z requires multiplication by 1.53, but the transformation of ρx is more complicated: $5.56 \text{ g/cm}^2 \cong 3.27 \text{ cm}$ in graphite, which when multiplied by 1.53 yields $5.0 \text{ cm} \cong 5.0 \text{ g/cm}^2$ in water.

Figure 14 illustrates the variation with mass depth, field size, and source distance, predicted by eq (7) using the reference values $z_g = 1.00 \text{ m}$, $\rho x_g^r = 5.0 \text{ g/cm}^2$, $f_g^r = 100 \text{ mm}$. The two curves show change in N_{graph} when either ρx_g or f_g is varied, with the other parameters held constant. The three points show that variation with distance alone is no larger than 0.15% over the range of distances covered here.

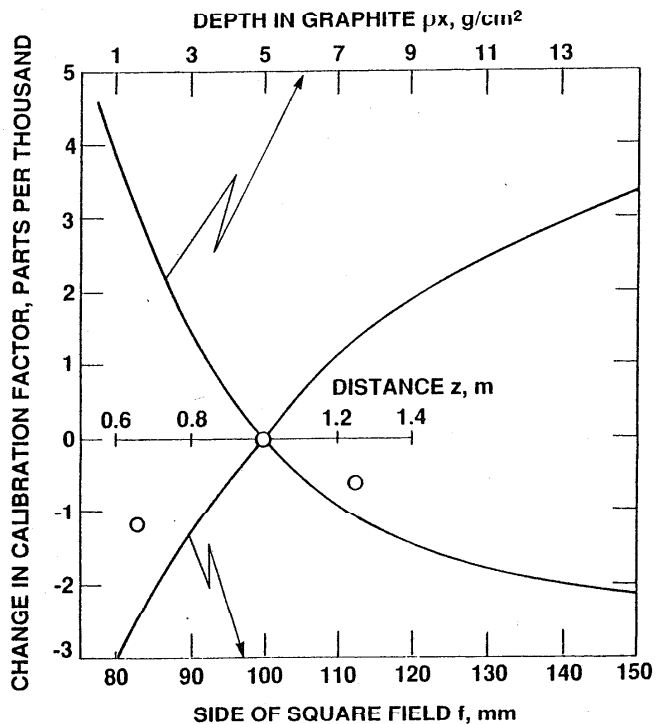


Figure 14. Dependence of PL1-type calibrations on depth in graphite phantom (top scale), and field size (bottom scale). The plotted points show dependence on source distance (middle scale).

Finally, figure 15 compares the measured calibration variation with source distance at a mass depth of $\rho x_g = 5.08 \text{ g/cm}^2$ and a collimator size $s = 33.4 \text{ mm}$ with the predictions of eq (7), using eq (6) to relate field size and collimator size. The agreement is excellent.

6. Calibration Transfer to Water

6.1 Theory

The following treatment is based on the general formalism described by Loevinger in 1981 [7]. Consider an ionization chamber immersed in an absorbing and scattering medium irradiated by ^{60}Co gamma rays. It is a thick-walled chamber so that all electrons reaching the cavity arise in the chamber walls rather than in the medium, which may be either graphite or water. The ratio of the mean absorbed dose rate in the chamber cavity air when the medium is graphite to the mean absorbed dose rate in the cavity air when the medium is water, is:

$$\frac{\dot{D}_{\text{air}}^{\text{graph}}}{\dot{D}_{\text{air}}^{\text{water}}} = \frac{I_{\text{air}}^{\text{graph}}}{I_{\text{air}}^{\text{water}}} \quad (8)$$

where I represents chamber current. In this notation the superscripts refer to the material of the media and the subscripts to the local chamber materials.

In each medium the cavity air absorbed dose rate can be related to the dose rate in the chamber wall material (if the cavity is filled with wall material) by using the Bragg-Gray equation [8]:

$$\frac{\dot{D}_{\text{wall}}^{\text{graph}}}{\dot{D}_{\text{air}}^{\text{graph}}} = \left(\frac{\bar{S}/\rho_{\text{wall}}}{\bar{S}/\rho_{\text{air}}} \right)^{\text{graph}}, \quad \frac{\dot{D}_{\text{wall}}^{\text{water}}}{\dot{D}_{\text{air}}^{\text{water}}} = \left(\frac{\bar{S}/\rho_{\text{wall}}}{\bar{S}/\rho_{\text{air}}} \right)^{\text{water}} \quad (9)$$

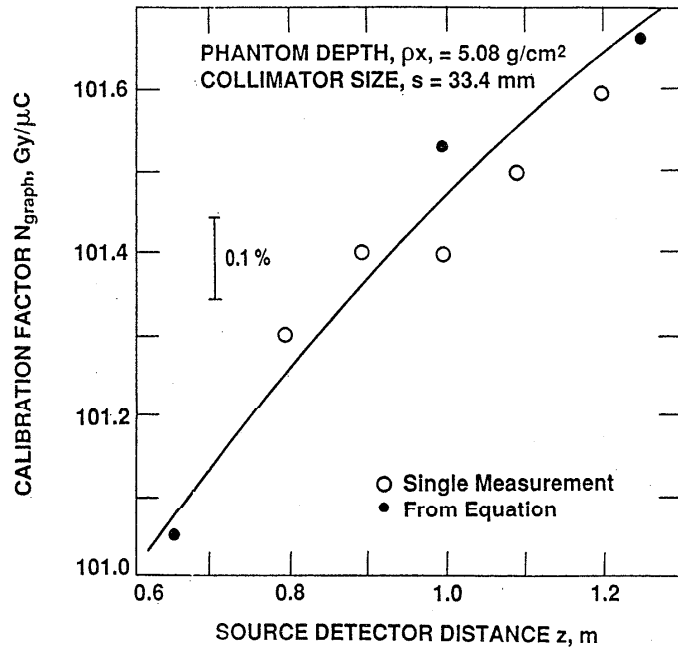


Figure 15. Comparison of measured and predicted (eq (7)) PL1-11 graphite phantom calibrations at several source distances and a fixed phantom depth. The line is drawn arbitrarily to fit the points.

where \bar{S}/ρ represents an electron mass stopping power averaged over the spectrum of electrons reaching the cavity. The positions of the chamber in the two media are always chosen so that source distances and depths are inversely proportional to the electron densities in the media. Under these conditions the relative spectra of photons and electrons at the cavity are the same [9] (also see Appendix A) and the stopping power average ratios are the same in graphite and in water.

Then from (9):

$$\frac{D_{\text{wall}}^{\text{graph}}}{D_{\text{air}}^{\text{graph}}} = \frac{D_{\text{wall}}^{\text{water}}}{D_{\text{air}}^{\text{water}}} \quad (10)$$

and substituting in (8):

$$\frac{D_{\text{wall}}^{\text{graph}}}{D_{\text{wall}}^{\text{water}}} = \frac{I_{\text{air}}^{\text{graph}}}{I_{\text{air}}^{\text{water}}} \quad (11)$$

Next, consider the ionization chamber (with its cavity filled with wall material) in the water medium. The ratio of the absorbed dose rate to water at the center of the chamber position with the chamber removed to the absorbed dose rate to the wall material at the center of the chamber position with the chamber present is:

$$\frac{D_{\text{water}}^{\text{water}}}{D_{\text{wall}}^{\text{water}}} = \frac{(\beta \bar{\mu}_{\text{en}}/\rho)_{\text{water}}}{(\beta \bar{\mu}_{\text{en}}/\rho)_{\text{wall}}} \times \frac{\psi_{\text{water}}}{\psi_{\text{wall}}} \quad (12)$$

where β is the ratio of absorbed dose to the collision part of kerma, and $\bar{\mu}_{\text{en}}/\rho$ is a mean mass energy-absorption coefficient for the photon spectrum at the chamber center position. The factor $\psi_{\text{water}}/\psi_{\text{wall}}$ is the ratio of photon fluence at the center position without/with the chamber present and corrects for the increased attenuation of the chamber compared to water.

Eliminating $D_{\text{wall}}^{\text{water}}$ from (11) and (12) and rearranging terms:

$$D_{\text{water}}^{\text{water}} = I_{\text{air}}^{\text{water}} \times \frac{\beta_{\text{water}}}{\beta_{\text{wall}}} \times \frac{(\bar{\mu}_{\text{en}}/\rho)_{\text{water}}}{(\bar{\mu}_{\text{en}}/\rho)_{\text{wall}}} \times \frac{\psi_{\text{water}}}{\psi_{\text{wall}}} \times \left(\frac{D_{\text{wall}}^{\text{graph}}}{I_{\text{air}}^{\text{graph}}} \right) \quad (13)$$

which is the water calibration equation. It describes how the absorbed dose rate in water with no chamber present ($D_{\text{water}}^{\text{water}}$) can be calculated from a chamber current measured in water ($I_{\text{air}}^{\text{water}}$), a measured chamber calibration in graphite ($D_{\text{wall}}^{\text{graph}}/I_{\text{air}}^{\text{graph}}$), absorbed-dose-to-kerma ratios ($\beta_{\text{water}}/\beta_{\text{wall}}$), a ratio of average mass energy-absorption coefficients [$(\bar{\mu}_{\text{en}}/\rho)_{\text{water}}/(\bar{\mu}_{\text{en}}/\rho)_{\text{wall}}$], and a measured fluence ratio ($\psi_{\text{water}}/\psi_{\text{wall}}$). For the particular chamber used here the wall material is graphite, but this equation can be applied to other wall materials.

6.2 Evaluation of the Coefficients

The ratio of absorbed dose to kerma does not differ by more than a few tenths of one percent for different materials [7], so that the ratio ($\beta_{\text{water}}/\beta_{\text{wall}}$) will be taken to be unity, with an uncertainty of 0.1 percent.

The mass energy-absorption coefficients for graphite and for water were taken from Hubbell [10] as a function of photon energy. They were averaged over photon energy using photon spectra predicted by Bruce and Johns [11] for ^{60}Co radiation incident on a water phantom, and photon spectra predicted by Seltzer et al. [12] for ^{50}Co radiation incident on a carbon phantom. If $P(k,x)$ represents a spectral distribution, where k is photon energy and x is depth in the phantom, the ratio of average mass energy-absorption coefficients is:

$$R_{\mu} = \frac{(\bar{\mu}_{\text{en}}/\rho)_{\text{water}}}{(\bar{\mu}_{\text{en}}/\rho)_{\text{wall}}} = \frac{\int_0^{\infty} (\mu_{\text{en}}/\rho)_{\text{water}} \cdot k P(k,x) dk}{\int_0^{\infty} (\mu_{\text{en}}/\rho)_{\text{wall}} \cdot k P(k,x) dk} \quad (14)$$

where the (μ_{en}/ρ) come from Hubbell. The same spectrum is used in both numerator and denominator of this ratio [9]. The Bruce-Johns predictions cover a range of water depths and three field sizes, as listed in Table 6A. The Seltzer predictions are for a fixed geometry, and are listed in Table 6B as a function of water depth and field size. (Seltzer assumed a graphite density of 1.80 g/cm², which transforms into an electron density of 1.62 relative to water, so that spectra at a depth of x_g in graphite are similar to spectra at a depth of $1.62 x_g$ in water.) It can be shown by interpolation of the Bruce-Johns data that their predictions differ by no more than a few tenths of one percent from those of Seltzer. The ratios used come from the matrix equation:

$$R_{\mu} = \sum_{i=0}^2 \sum_{j=0}^2 f_w^i M_{ij} x_w^j \quad (15)$$

where f_w is field size in water in mm and x_w is water depth in mm. The matrix components, M_{ij} , are listed in table 6C. Equation (15) generates the values of R_{μ} listed in table 6B to within 0.02% and those listed in table 6A to within 0.25%. The variation with both x_w and f_w is shown to be almost negligible in figure 16.

Table 6. Ratio of average mass energy-absorption coefficients, $(\bar{\mu}_{\text{en}}/\rho)_{\text{water}}/(\bar{\mu}_{\text{en}}/\rho)_{\text{wall}}$, as a function of water depth x_w and field size f_w

6A Calculated using Bruce-Johns spectra

x_w , mm	$f_w = 50$ mm	100 mm	200 mm
0	1.11078	1.11095	1.11118
20	1.11088	1.11109	1.11152
50	1.11097	1.11128	1.11195
100	1.11114	1.11157	1.11251
200	1.11107	1.11166	1.11300

6B Calculated using the spectra of Seltzer et al.

x_w , mm	f_w , mm	R_μ
11.3	115.6	1.11171
27.5	116.6	1.11198
50.2	118.1	1.11243
76.1	119.8	1.11294
102.1	121.5	1.11349
124.7	123.0	1.11366

6C Matrix components

$$\begin{array}{lll}
 M_{00} = 1.11104 & M_{01} = 1.50 \text{ E-5} & M_{02} = -2.53 \text{ E-8} \\
 M_{10} = 5.10 \text{ E-6} & M_{11} = 3.21 \text{ E-9} & M_{12} = 1.88 \text{ E-10} \\
 M_{20} = -1.12 \text{ E-8} & M_{21} = 3.50 \text{ E-10} & M_{22} = -1.61 \text{ E-12}
 \end{array}$$

The fluence ratio $\psi_{\text{water}}/\psi_{\text{wall}}$ (called here a "replacement factor") was determined from replacement measurements made with three nesting graphite sleeves. These were 10-cm long and fitted on the outside of the acrylic tube spanning the water phantom described in section 4. With the phantom filled with water and a PL1 graphite chamber inside the tube, measurements were made of the decrease in current when the water surrounding the acrylic tube was replaced by graphite sleeves with total wall thicknesses of 2.5, 5.1, and 7.6 mm. Any graphite sleeves not being used were pushed out of the beam but were still underwater, so that the water depth remained constant.

These measurements are plotted as a function of wall thickness in figure 17 (which also shows similar measurements made with acrylic and polystyrene nesting sleeves). Replacement of water by graphite reduces the chamber current by 0.156% per mm of wall thickness, or 0.078% per mm increase in diameter. By extrapolation, it follows that replacement of water by a graphite rod 12.3 mm in diameter (the PL1 chamber) would decrease the central fluence by 0.96%, so that $\psi_{\text{water}}/\psi_{\text{wall}} = 1.0096$.

The replacement measurements for graphite and acrylic are summarized in DB 810/132. Those for polystyrene are in DB 827/164-168. It should also be mentioned here that a footnote in reference [1] is misleading. This footnote states that the published replacement correction factor, 0.068% per mm, has been corrected for the difference between the average graphite phantom density and the graphite sleeve density. It can be seen from eq (12) above that the replacement factor does not involve the graphite phantom, and since the sleeves and chambers were made from the same graphite rod, no density change correction was needed.

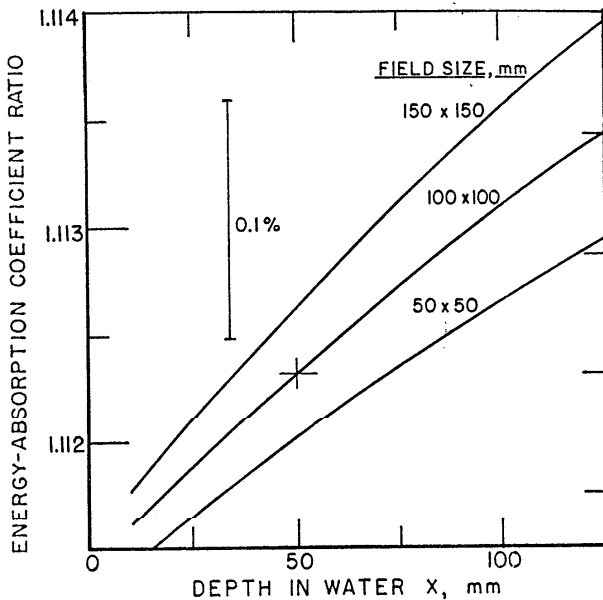


Figure 16. Ratio of mean mass energy-absorption coefficients of water and of graphite as a function of field size and depth in a water phantom.

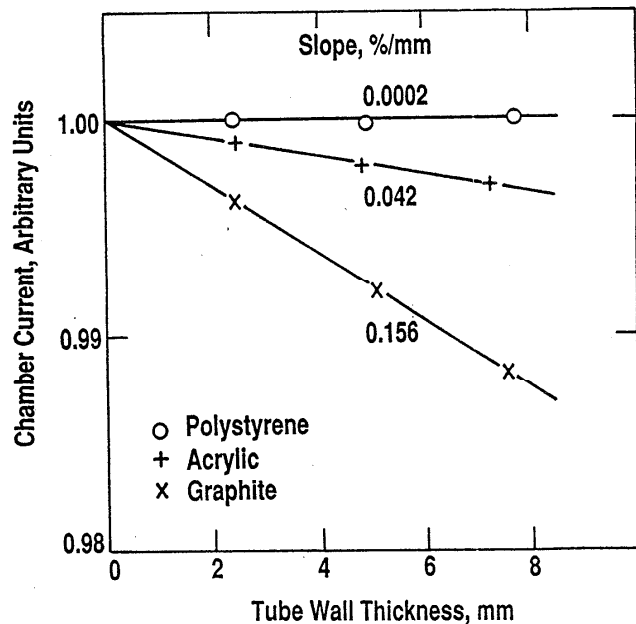


Figure 17. Measurements of replacement factors obtained by sliding tubes of polystyrene, acrylic plastic, and graphite over PL1-11 in the water phantom.

6.3 The Chamber Currents in Water

The water currents were measured with chamber PL1-11 as a function of depth, x_w , and collimator size, s , in a series of five experiments performed between 1978 October 27 and 1982 February 3. The currents listed in table 7A have all been corrected for:

- (a) air density changes inside the chamber, using the correction factor $[101.325(T + 273.15)/(295.15 P)]$, where T is air temperature in degrees Celsius and P is air pressure in kilopascals,
- (b) source decay from $t = 0$ on 1979 Jan 1, using the correction factor $\exp(0.0003600 t)$, where t is time in days,
- (c) telethermometer errors, using a correction factor ranging from 1.0004 (DB 801/148-149) to 1.0006 (DB 827/63).
- (d) digital voltmeter errors ranging from 0.9990 (DB 827/60) to 0.9992 (DB 827/173) to 1.0009 (DB 810/7).
- (e) extra attenuation of the acrylic tube, using the correction factor 1.0006, which comes from the replacement measurements of figure 17.

The original current measurements can be found in DB 810/52-54 for experiment #1, in DB 812/127-129 for experiment #2, in DB 812/188-191 for experiment #3, in DB 827/76 for experiment #4, and in DB 827/170-171 for experiment #5. Of the original data only the capacitance values, the measured voltage changes, and the measured values of correction (a) were retained.

6.4 The Absorbed Dose Rate in Water

The absorbed dose rate in a water phantom comes from eq (13), which may be rewritten:

$$\dot{D}_w(x_w, f_w) = 1.0096 R_\mu(x_w, f_w) I(x_w, s) \frac{\dot{D}}{I}(x_g, f_g) \quad (16)$$

where $\dot{D}_w(x_w, f_w) = \dot{D}_{\text{water}}$, $I(x_w, s) = I_{\text{air}}^{\text{water}}$, $\frac{\dot{D}}{I}(x_g, f_g) = \frac{\dot{D}_{\text{wall}}^{\text{graph}}}{I_{\text{air}}^{\text{graph}}}$, and R_μ comes from eq (15) and table 6C. What remains to be done is to rewrite $\frac{\dot{D}}{I}(x_g, f_g)$ as a function of x_w and f_w . This can be done by scaling source distances, field sizes, and phantom depths inversely with electron densities. It is shown in reference [9] that if this is done, photon spectra will have the same relative shapes in different materials, so that eq (10) is valid, and consequently, eqs (13) and (16) are also valid.

Table 7. Current from chamber PL1-11 and absorbed dose rate to water at 1 m as a function of depth in water, x_w , and collimator size, s . Currents are corrected to 22°C and 1 atm. Currents and dose rates are both corrected to 1979 Jan 1.

Water depth x_w mm	7A PL1-11 current $I(x_w, s)$, nA				7B Dose rate to water $\dot{D}(x_w, s)$, mGy/s			
	$s=28.0$ mm	33.4 mm	40.5 mm	50.8 mm	$s=28.0$ mm	33.4 mm	40.5 mm	50.8 mm
9.6	0.1926			0.2051	21.94			23.50
10.9	0.1922	0.1962	0.2002	0.2047	21.89	22.39	22.89	23.45
12.4		0.1954				22.29		
21.4	0.1868	0.1911	0.1954	0.2002	21.22	21.76	22.29	22.87
31.7		0.1842				20.94		
35.0	0.1777	0.1823	0.1870	0.1923	20.15	20.71	21.29	21.93
36.3	0.1765	0.1814	0.1861	0.1914	20.01	20.61	21.19	21.83
45.9		0.1750				19.85		
47.4	0.1683			0.1845	19.06			21.01
51.8	0.1654	0.1709	0.1760	0.1817	18.73	19.38	20.00	20.69
53.5		0.1689				19.16		
59.9	0.1593	0.1646	0.1701	0.1761	18.02	18.66	19.32	20.05
61.4		0.1636				18.55		
67.3	0.1536	0.1593	0.1648	0.1711	17.37	18.05	18.72	19.47
73.9		0.1538				17.43		
81.5	0.1428	0.1488	0.1545	0.1612	16.14	16.85	17.53	18.33
85.5	0.1399	0.1456	0.1515	0.1583	15.81	16.49	17.20	18.00
94.2		0.1389				15.72		
96.1	0.1322	0.1384	0.1442	0.1511	14.94	15.67	16.36	17.17
96.5	0.1314			0.1504	14.86			17.10
104.6	0.1261	0.1318	0.1379	0.1450	14.25	14.92	15.65	16.48
114.7		0.1245				14.10		

The number of electrons per cm³ in graphite with a mass density of 1.70 g/cm³ is $1.70 \times 6 N_A / 12.011 = 0.8492 N_A$, where N_A is Avogadro's number. The electrons/cm³ in water with a mass density of 1 g/cm³ is $(2 \times 1 + 1 \times 8) N_A / (2 \times 1.0080 + 1 \times 16.0) = 0.5551 N_A$. The ratio of these is graphite/water = 1.53, so that the conditions will be satisfied if:

$$\begin{aligned} \text{source distance} \quad z_w &= 1.53 z_g \\ \text{field size} \quad f_w &= 1.53 f_g \\ \text{phantom depth} \quad x_w &= 1.53 x_g \end{aligned} \quad (17)$$

where the subscripts w and g refer to water and graphite, respectively.

As for the transformation of currents, this comes from eq (6), which in light of (17) can be rewritten:

$$\frac{f_g}{z_g} = \frac{f_w}{z_w} = 2.85 \text{ s} \quad (18)$$

This shows that although field size and source distance transform according to eq (17), collimator size, s, is invariant. That is, photon spectra at points (z_w, x_w, f_w) in a water phantom are similar to photon spectra at points (z_g, x_g, f_g) in a graphite phantom if the same collimator is used in each case.

The ratio $\dot{D}/I(x_g, f_g)$, which is the same as $N_{\text{graph}}(x_g, f_g)$, can, in light of (7) and (17), be rewritten as:

$$N_{\text{graph}}^{\text{ref}} [1 + k_x (1 - \exp[-\xi_x (x_w - 50)]) + k_f (1 - \exp[-\xi_f (f_w - 100)])] \quad (19)$$

with both x_w and f_w in mm. This equation is to be used at a source distance of $z_w = 1$ m, so the parameters $N_{\text{graph}}^{\text{ref}}$, k_x , k_f , ξ_x , and ξ_f must all be transformed from the corresponding graphite parameters for a source distance of $z_g = 1/1.53 = 0.654$ m. Then, from table 5, $N_{\text{graph}}^{\text{ref}} = 101.07 \text{ Gy}/\mu\text{C}$, $k_x = -0.00333$, $k_f = 0.00595$, $\xi_x = 0.0278 \text{ mm}^{-1}$, and $\xi_f = 0.0164 \text{ mm}^{-1}$. (Equation (19) for water at $z_w = 1.00$ m will track eq (7) for graphite at $z_g = 0.654$ m only if k_x and k_f remain unchanged and if $5.56 \gamma_x = 50 \xi_x$ and $65.4 \gamma_f = 100 \xi_f$.)

Then, putting (19) into (16), the dose rate to water at a source distance of 1 m is:

$$\begin{aligned} \dot{D}_w(x_w, f_w) &= 1.0096 R_{\mu}(x_w, f_w) I(x_w, f_w) N_{\text{graph}}^{\text{ref}} [1 + k_x (1 - \exp[-\xi_x (x_w - 50)]) \\ &\quad + k_f (1 - \exp[-\xi_f (f_w - 100)])] \text{ mGy/s} \end{aligned} \quad (20)$$

For a particular collimator size, s , the field size f_w comes from (18). The currents $I(x_w, f_w)$ are measured at 1 m with chamber PL1-11 and are corrected to 22 °C and 1 standard atmosphere pressure.

The calculated dose rates for the currents listed in table 7A are shown in table 7B. They refer to 1979 Jan 1. For each collimator size, the water absorbed dose rates at 1 m have been fitted to an equation of the type:

$$\dot{D}_w(x_w, s) = \left(\sum_{i=0}^3 C_i(s) x_w^i \right) \exp(-0.01 x_w) \text{ mGy/s} \quad (21)$$

The coefficients $C_i(s)$ are listed as a function of s in table 8 along with coefficients of variation, V . As can be seen, the coefficients of variation are all smaller than 0.2%.

Table 8. Coefficients $C_i(s)$ in water absorbed-dose rate eq (21), on 1979 Jan 1. The coefficient of variation, V , was calculated for 4 degrees of freedom.

Coefficients	Collimator size, mm			
	28.0	33.4	40.5	50.8
c_0	22.45	22.99	23.46	23.99
c_1	0.1819	0.1828	0.1911	0.1975
c_2	-2.49E-4	-0.16E-4	0.37E-4	1.62E-4
c_3	1.57E-6	0.45E-6	0.62E-6	0.42E-6
$V, \%$	0.12	0.18	0.09	0.08

Finally, the calibration of PL1-11 in a water phantom at 1 m is the ratio $\dot{D}_w(x_w, f_w)/I(x_w, f_w)$, or

$$N_{\text{water}}(\text{PL1-11}) = 102.04 \left(\sum_{i=0}^2 \sum_{j=0}^2 f_w^i M_{ij} x_w^j \right) [1 - 0.00333(1 - \exp[-0.0278(x_w - 50)]) + 0.00595(1 - \exp[-0.0164(f_w - 100)])] \text{ Gy}/\mu\text{C} \quad (22)$$

at 22 °C and 1 standard atmosphere, where the matrix elements M_{ij} come from table 6C. Both x_w and f_w are in millimeters, and $z_w = 1$ meter.

7. Operational Procedures

7.1 Exposure Techniques for Various Chambers

We have calibrated several types of ionization chambers for determination of absorbed-dose rate in a ^{60}Co gamma-ray beam. In general, these can be divided into two types, thimble chambers and flat chambers. The thimble chambers, which include our own PL1 chambers, have been inserted into the plastic tube of the water phantom. At the time of writing (April 1989) four calibration reports have been issued for customer-owned thimble chambers. Two of the chambers were Exradin model A-1 chambers (SN 151 and 153), one was a Farmer probe, model 2505/3 (SN 1400), and one was a 1-cm³ E.G.&G. model (SN 43-A). The first three were placed in the 12.7 mm I.D. tube and compared with chamber PL1-11 at water depths of about 50 mm, and a source distance of 1 m. In each case, the chamber was fitted with an acrylic adapter so that the tube was filled with plastic rather than air. For the larger diameter E.G.&G. chamber, the 12.7-mm I.D. plastic tube was replaced by a 19.1-mm I.D. tube and again a special adapter was used to fill the tube with acrylic. In all cases, the calibration consisted of measuring the ratio of PL1-11 current to current from the customer-owned chamber, for the same measurement conditions, and multiplying by the appropriate PL1-11 calibration factor from eq (22):

$$N_{\text{water}}(\text{customer}) = \frac{I(\text{PL1-11})}{I(\text{customer})} \times N_{\text{water}}(\text{PL1-11}) \quad (23)$$

where I is current.

When the customer-owned chamber fits in the 12.7-mm I.D. tube, with its adapters, the exposure of PL1-11 in the same tube is performed using a passive graphite rod to fill the rest of the tube. When the 19.1-mm I.D. tube must be used, PL1-11 and its passive rod are surrounded by an acrylic sleeve to eliminate air pockets from the tube. Acrylic sleeves attenuate the photons more than water does and this can be compensated for by multiplying the measured current by $(1 + 0.00042 t_{\text{wall}})$, where t_{wall} is the wall thickness of the acrylic sleeve in millimeters. The coefficient comes from figure 17.

Most of the flat chambers calibrated here are model MPPK, manufactured by Memorial Hospital in New York City.⁴ These are plane-parallel chambers 4.5 cm in diameter and 1-cm thick, consisting of two conducting plastic discs, each 4-mm thick, separated by a 2-mm air gap. The chamber is centered in a 25-cm x 25-cm x 1-cm thick polystyrene plate which can form part of a 25-cm square polystyrene phantom. The phantom used in this laboratory consists of two 25-cm square polystyrene plates, each 6-mm thick, and a 30-cm diameter polystyrene block, 10-cm thick. During calibration, the flat chamber plate is sandwiched between the two 6-mm plates with the one labeled PST on top and the one labeled PSB on the bottom. The entire sandwich sits on top of the

⁴We have also calibrated a Capintec model PS-033, which differs in detail, but for which the calibration techniques are similar.

30-cm diameter block, which acts as a backstop. The reference plane in the chamber coincides with the inside surface of the top electrode, 4 mm below the top of the chamber and its surrounding polystyrene plate. The chamber is calibrated at two polystyrene depths, 4 mm, with the plate PST removed, and 10 mm, with the plate PST in place.

Comparison with PL1-11 is made by removing the flat chamber sandwich and placing PL1-11 with its passive graphite rod in a 12.7-mm diameter hole across the 30-cm diameter block. The central axis of this hole is 9.5 mm below the top surface of the block. (During calibration of the flat chamber, this hole is either filled with a plastic rod or effectively removed by turning over the block.) The source distances are adjusted so that both the central axis of PL1-11 during its use and the reference plane defined above for the flat chamber are at a source distance of 0.984 meter [9]. This distance was chosen so that photon and electron spectra would be the same in polystyrene as at a source distance of 1.00 m in water, transforming inversely with electron density as in section 6.4. The number of electrons per cm³ in polystyrene with a mass density of 1.049 g/cm³ is $1.049 \times 7 N_A / 13.019 = 0.5640 N_A$, which is $1/0.984 = 1.016$ times the electron density in water, $0.5551 N_A$, where N_A is Avogadro's number.

The calibration equation for flat chambers is more complicated than eq (23) because the PL1-11 current and the flat chamber current are measured at slightly different depths in polystyrene. Equation (23) can be replaced by the more general equation:

$$N_{\text{water}}(\text{customer}) = \frac{\dot{D}(\text{customer})}{\dot{D}(\text{PL1-11})} \times \frac{I(\text{PL1-11})}{I(\text{customer})} \times N_{\text{water}}(\text{PL1-11}) \quad (24)$$

where the added \dot{D} terms are absorbed dose rates to water at the chamber positions with the chambers removed. When the water phantom is used with thimble chambers, both PL1-11 and the customer chamber are placed in the same position, and (24) reduces to (23). In the flat chamber case, the ratio $\dot{D}(\text{customer})/\dot{D}(\text{PL1-11})$ can be evaluated from eq (21) and table 8, where it must be remembered that x_w is a distance in water, which is $1.016 x_p$, if x_p is in polystyrene. For the present case, using a collimator size of $s = 33.4$ mm, the predicted dose rates to water on 1979 Jan 1 at depths of 1.016×4 mm, 1.016×9.5 mm, and 1.016×10 mm are 22.79, 22.48, and 22.45 mGy/s, respectively. Then the ratio $\dot{D}(\text{customer})/\dot{D}(\text{PL1-11})$ is $22.79/22.48 = 1.014$ with plate PST absent (polystyrene depth = 4 mm) and $22.45/22.48 = 0.999$ with PST present (polystyrene depth = 10 mm).

7.2 Current Measurements and Corrections

The collecting electrode of the ionization chamber being studied is connected via low-noise coaxial cable to the input of a Keithley 610C electrometer. This instrument has a dial readout that is usually turned off. In its place, a Digitec 266 DC voltmeter (DVM) provides a digital readout of the electrometer feedback voltage. The X1 Output of the 610C is connected to the Hi terminal of the DVM, and the Guard terminal of the 610C is connected to the Lo terminal of the DVM. The 610C is used with the Feedback switch set to fast, and the mode switch set to 10^{-8} , 10^{-9} , or 10^{-10} coulombs full scale.

The electrometer is used with a locally made DVM timer, which controls the Digitec DVM display. The timer output is connected to terminals D6 on the DVM card-edge connector, so that the DVM displays the instantaneous electrometer feedback voltage only when it gets a positive pulse from the timer. The front panel of the timer contains an ERC counter, an ITC comparator, and a Start button. When the Start button is pushed, the timer generates a pulse, the DVM displays an initial voltage, and the counter starts counting elapsed time. When the counter reaches the pre-set comparator number, it generates a second pulse, the DVM displays a final voltage, and the counter stops counting. For the timer usually used, the time unit for both counter and comparator is centiseconds. (For some of the local DVM timers, the time unit is milliseconds.)

High voltage for the chamber is provided by a Keithley model 240A power supply, capable of generating from 0 to 1200 V of either polarity. Measured ionization currents are corrected to 22 °C and 1 atm (101.325 kPa = 1013.25 mbar = 760 mmHg). Pressure measurements are made with a Wallace and Tiernan FA139 aneroid barometer and temperature measurements with a Digitec 5810 thermistor thermometer.

The chamber current measured in amperes during a run is:

$$I = C \times \frac{V_F - V_I}{\Delta t} \quad (25)$$

where: C is the electrometer capacitance, in farads:

V_I and V_F are the initial and final DVM measurements, in volts;
 Δt is the run time, in seconds, determined by the DVM timer.

The value of the capacitance C must be determined for each electrometer scale by independent measurements. For the particular electrometer usually used, NBS #184539, the capacitances measured in December 1987 were:

Full-scale (C)	Capacitance (pF)
10 ⁻⁸	10,003.
10 ⁻⁹	1,012.5
10 ⁻¹⁰	104.02

(These numbers have changed by less than 0.1% from earlier measurements in 1982.)

A fully corrected current in a polystyrene phantom at a source distance of 0.984 m can be written as:

$$I_C = (I - I_L) \times [101.325(273.15+T)/(295.15 P)] \times (0.984)^2 \times C_D \times C_{PT} \quad (26)$$

where I is current measured during irradiation, I_L is leakage current measured with no radiation incident, T is temperature in degrees Celsius, P is pressure in kPa, C_D is a correction for systematic errors in the DVM, and C_{PT} is a correction for systematic errors in the temperature and pressure measurements.

The term in square brackets is the correction to a reference air density, and the $(0.984)^2$ term corrects the current to a source distance of 1 m in a water phantom.

Ordinarily, if I_L is negligible, $I_C(\text{PL1-11})/I_C(\text{customer})$ is equal to $I(\text{PL1-11})/I(\text{customer})$, since most of the factors cancel out, but the measured currents should be fully corrected anyway, for the purposes of Quality Assurance, as described below.

7.3 Quality Assurance Measurements

These consist of following the measurements of $I_C(\text{PL1-11})$ in the 30-cm diameter polystyrene block and fitting them to the equation:

$$I_C = A e^{-\alpha t} \quad (27)$$

where t is the number of days since 1979 Jan 1 and $\alpha = 0.0003600 \text{ day}^{-1}$ [4]. These measurements yield values of A in (27). The block consists of four 30-cm diameter polystyrene plates taped together (labeled PB1, PA4, PA5, and PA6 in DB 827/65) with a total thickness of 9.3 cm. A 12.7-mm hole was drilled along a diameter 9.5 mm below the top surface of the block. During QA measurements, the axis of symmetry of the block coincides with the beam axis and the axis of the hole is 0.984 m from the source. PL1-11 and its passive graphite backstop fill the hole, with the beam axis passing through the chamber at a point 6.6 mm from the square end. No extra absorbers are added atop the block. Currents are measured and corrected as described in section 7.2.

To date (October 1989) there have been five reliable measurements of I_C covering a span of more than 6 years. The data are listed in table 9A. The values of C_D and C_{PT} used to obtain I_C in each case are shown in columns 4 and 5, along with the databook references in parentheses. Table 9B shows the calculated zero-time amplitudes $A = I_C \exp(\alpha t)$, plus deviations from the average. These deviations are all less than 0.2% in absolute magnitude, providing assurance that the calibration quality has remained high.

7.4 Chamber MPPK-281

The NBS purchased a flat Memorial Hospital chamber (MPPK-281) in 1985. In each flat chamber calibration since then, comparison with MPPK-281 has been included with comparison of PL1-11 in the 30-cm polystyrene block and the customer's flat chamber. The average ratio of MPPK-281 current to PL1-11 current during the three most recent calibrations is $3.595 \pm 0.17\%$ (DB 843/41). It is hoped that continued use of MPPK-281 with PL1-11 will result in a reliable calibration of MPPK-281, which will enable PL1-11 to be eliminated from flat chamber calibrations.

At the same time, the comparison of PL1-11 and other thimble chambers in the polystyrene block is much more convenient than their comparison in the water phantom. It is proposed to use this block, with additional polystyrene plates added on top, to calibrate all thimble chambers that will fit in the 12.7 mm diameter hole in that block, using the methods described above.

Table 9. Corrected PL1-11 current in polystyrene block at source distance 0.984 m, phantom depth 9.5 mm, collimator size 33.4 mm, at 22 °C and 1 atm

9A As a function of time, t, measured from 1979 Jan 1

Number	Date	Reference	C _D (DB)	C _{P_T} (DB)	Current I _C , nA	Time t, days
1	81 Apr 2	DB 827/69	0.9990(827/60)	1.0006(827/63)	0.14597	823
2	82 Oct 21	843/1	0.9990(827/60)	1.0006(827/63)	0.11876	1390
3	84 Mar 8	843/17	0.9985(843/8)	1.0006(827/63)	0.09908	1894
4	87 Mar 24	843/37	0.9990(843/36)	1.0006(827/63)	0.06640	3005
5	87 Dec 4	843/40	0.9990(843/36)	1.0006(827/63)	0.06054	3260

9B Calculation of zero-time amplitude A.

Number	A, nA	A-A _{mean} (%)
1	0.19631	+ 0.18
2	0.19588	- 0.04
3	0.19593	- 0.01
4	0.19588	- 0.04
5	0.19576	- 0.10
Mean	0.19595 ± 0.1%(m.e.)	

8. Calibration Uncertainties

The absorbed dose calibration of chamber PL1-11 can be transferred to another (secondary) chamber by substitution in a water phantom in the ⁶⁰Co gamma-ray beam. The component uncertainties that enter into the absorbed dose rate to water (eq (16)) and into the calibration of the secondary chamber are given in table 10. Conventional statistical estimates of random uncertainties are given as standard deviations of the mean, designated "type A," which can be considered to be objective estimates. All other uncertainty estimates, designated "type B," are subjective estimates, based on the experience of the calibration staff. The type B uncertainties are estimated as realistic upper bounds of the possible errors, and correspond very roughly to 99% confidence limits.

The overall uncertainty U comes from combining the type A uncertainties (s_i) and the type B uncertainties (w_i) by means of the equation:

$$U = 3\sqrt{\sum s_i^2 + \sum (w_i/3)^2} \quad (28)$$

where the terms (w_i/3)² are treated as variances [13]. This overall uncertainty then, corresponds roughly to a 99% confidence limit when the statistical uncertainties are included.

For the first three parts of table 10, the uncertainties are separated into those involved in the direct measurements of calorimeter power and PL1-11 chamber current, and those involved in the determination of the corrections. The correction factor uncertainties are listed separately in table 11. The numbers listed for correction factors in table 10 are $\sqrt{\sum w_i^2}$ where the w_i come from table 11. In table 11, five component uncertainties have been taken to be equal to zero, because the time interval between 1.(b) and 2.(bb) was negligible, the geometry is such that 1.(g) and 2.(ee) are equal, and the 1.(f) correction was not needed for the water calibration, for which only $z_g = 0.654$ m was used.

Table 10. Uncertainty Analysis

Component	Estimated uncertainty (%)	
	Type A s_i	Type B w_i
1. Calorimeter		
Power measurements	0.04	0.03
Correction factors		0.12
2. PL1-11 chamber in graphite		
Current measurements	0.03	0.05
Correction factors		0.11
3. PL1-11 chamber in water		
Current measurements	0.03	0.05
Correction factors		0.11
4. Dose rate conversion, graphite to water		
Absorption coefficient ratios		0.5
Replacement factor		0.2
β ratio		0.1
Positioning of chamber and calorimeter		0.1
Failure of PL1-11 wall buildup		0.15
Failure of scaling theorem		0.2
5. Chamber being calibrated		
Current measurements	0.1	0.1
Positioning of chambers		0.2
Overall uncertainties, U		
Absorbed dose rate to water (1 through 4)		0.7%
Secondary chamber calibration (1 through 5)		0.8%

As shown in table 10 the overall uncertainty in determining the absorbed-dose-rate to water is $\pm 0.7\%$, while that for calibrating any secondary chamber is $\pm 0.8\%$. In both cases, the main contribution comes from the $\pm 0.5\%$ uncertainty assigned to Hubbell's absorption coefficient ratios. His estimate of $\pm 0.3\%$ [10] applies to monoenergetic photons in the ^{60}Co energy range. As described in reference [1], this was arbitrarily increased to $\pm 0.5\%$ because of the presence of low-energy photons, for which the ratio is much less accurately known.

The uncertainty for calibration of secondary chambers in calibration reports can be conveniently rounded to $\pm 1\%$.

Table 11. Correction factor uncertainties

Component	Estimated Uncertainty % Type B w_i
1. Calorimeter corrections (section 5)	
(a) Excess ring scatter	0.02
(b) Source decay	0.00
(c) Shutter timer	0.01
(d) Core impurities	0.1
(e) Acrylic ring	0.02
(f) Protection air gap (only for $z_g=1.0$ m)	0.00
(g) Escaping radiation	0.00
(h) Core air gaps	0.05
2. PL1-11 graphite current corrections (section 5)	
(aa) Air density changes	0.1
(bb) Source decay	0.00
(cc) Telethermometer errors	0.02
(dd) Instrumental errors	0.04
(ee) Escaping radiation	0.00
(ff) Mass depth difference	0.01
3. PL1-11 water current corrections (section 6.3)	
(a) Air density changes	0.1
(b) Source decay	0.02
(c) Telethermometer errors	0.02
(d) Digital voltmeter errors	0.04
(e) Acrylic tube attenuation	0.02

APPENDIX A — Test of the Photon Fluence Scaling Theorem

The purpose of this appendix is to present the data on which the conclusions of reference [9] are based. Currents from ion chamber PL1-11 were measured in the ^{60}Co beam from the 10-kCi Theratron F source using phantoms of water, polystyrene, acrylic plastic, and graphite. These currents were measured as a function of depth in the phantoms for several source distances. These distances were chosen to test the theorem that for photons that interact with low-Z materials by means of the Compton effect, distances in these materials scale inversely with the electron densities, and photon fluences scale directly with the square of the electron densities.⁵

The measurement conditions are shown in table 12 which lists the mean mass densities and the electron densities relative to water for the four media used. Source-detector distances used in three separate experiments (A, B, and C) are also shown. In each of the three experiments, the product of source distance and relative electron density is the same for each medium. At each position, PL1-11 current was measured as a function of phantom depth, for the four field sizes determined by the 50.8-mm, 40.5-mm, 33.4-mm, and 28.0-mm collimator jigs (as summarized in DB 843/59-63).

Table 12. Test of scaling theorem; conditions and results

	Material			
	Water	Polystyrene	Acrylic	Graphite
Mean mass density, g/cm ³	1	1.049	1.182	1.70
Relative electron density	1	1.016	1.149	1.53
Source-detector distance, m	A 1.000	0.984	0.870	0.654
	B 1.265	1.245	1.101	0.827
	C 1.530	1.506	1.332	1.000
Total normalization factor	A 1.008	1.012	1.004	0.980
	B 1.022	1.024	1.016	0.995
	C 1.026	1.032	1.024	1.004
PL1-11 replacement factor	1.010	1.010	1.007	1.001

The current measurements were all corrected to a temperature of 22 °C, a pressure of 101.325 kPa, and a time zero of 1979 Jan 1. In addition, each current was multiplied by the square of the source distance, to correct it to a distance of 1 m, to a first approximation. When all of the corrected measurements for a given experiment and a given collimator jig were plotted as a function of scaled phantom depth (true phantom depth × electron density of

⁵Electron density as used here means electrons per unit volume.

phantom/electron density of water), it was found that the curves for water, polystyrene, acrylic, and graphite were always very similar in shape but displaced in magnitude by as much as a few percent.

It was found by trial and error that if the corrected currents were multiplied by the total normalization factors listed in table 12 as a function of experiment and material, this displacement in magnitude could be reduced to a few tenths of one percent. The normalized currents are listed in table 13, where the units were nanoamperes before normalization. Also shown in table 13 are the least-squares polynomial coefficients in the equation:

$$I_p(x) = \left(\sum_{i=0}^3 b_i x^i \right) \exp(-0.01 x) \quad (29)$$

where x is scaled phantom depth in mm. The coefficients of variation of the fits, V , are also listed in percent in table 13. The curve-fitting residuals, $(I - I_p)$ are shown in percent in figure 18 for these 12 curves. The most striking systematic variation is for the graphite residuals, which all have the same general shape and the largest deviations. In general, the normalized depth-current curves agree to within a few tenths of one percent, and the scaling theorem appears to work within that limit.

The normalization factors of table 12 are not unity for several reasons. First, with the ion chamber at different distances from the source, there will be different amounts of air attenuation. The measurements can be corrected for air attenuation by multiplying by the factor $(1 + 0.0032 z)$, where z is source distance in meters, and 0.0032 m^{-1} comes from the mass energy-absorption coefficient for air at a photon energy of 1.17 MeV [10] and the density of air at 22 °C.

Second, the measurements can also be corrected for replacement of the graphite chamber by phantom material, using the replacement factors listed in table 12. These were calculated from the data of figure 17, using the following reasoning:

As in the evaluation of $\psi_{\text{water}}/\psi_{\text{wall}}$ in section 6.2, it can be deduced from figure 17 that insertion of a 12.3-mm diameter rod (the same size as the chamber) in a water phantom reduces the central axis fluence by a factor of 1/1.0000 if the rod is polystyrene, by a factor of 1/1.0026 if the rod is acrylic, or by a factor of 1/1.0096 if the rod is graphite. Replacing a graphite rod by an acrylic (or polystyrene) rod may be done in two steps. Replacing a graphite rod by a water rod increases the fluence by the factor 1.0096 (hence the 1.010 replacement factor for water). Replacement of the water rod by an acrylic (or polystyrene) rod decreases the fluence by a factor of 1/1.0026 (or 1/1.0000). Thus, replacement of a graphite rod by an acrylic (or polystyrene) rod increases the fluence by a net factor of $1.0096/1.0026 = 1.0070$ (or $1.0096/1.0000 = 1.0096$), giving the table 12 replacement factor of 1.007 (or 1.010).

Table 13. Normalized PLI-11 currents in 4 phantoms during 3 experiments, plus polynomial coefficients for eq (29) in text. The coefficient of variation, V, was calculated for 4 degrees of freedom.

Scaled phantom depth, mm	Experiment A				Experiment B				Experiment C																											
	Collimator Size, mm																																			
	50.8	40.5	33.4	28.0	50.8	40.5	33.4	28.0	50.8	40.5	33.4	28.0																								
Water Phantom																																				
8.8	0.2013	0.1966	0.1922	0.1879	0.2094	0.2047	0.2004	0.1961	0.2032	0.2001	0.1930	0.1912																								
21.4																																				
22.2																																				
23.5																																				
28.1																																				
28.3																																				
30.6					0.1992	0.1939	0.1891	0.1843																												
36.3					0.1925	0.1873	0.1825	0.1775																												
49.1					0.1828	0.1771	0.1719	0.1664					0.1860	0.1801	0.1747	0.1693	0.1851	0.1826	0.1802	0.1692																
51.8																																				
53.0																																				
53.2																																				
56.2																																				
59.0																																				
67.3																					0.1721	0.1658	0.1602	0.1545												
74.5																					0.1621	0.1554	0.1497	0.1436	0.1719	0.1653	0.1595	0.1538	0.1630	0.1561	0.1620	0.1453				
76.2																																				
81.5																																				
90.5																																				
93.2																																				
93.6																																				
96.1	0.1519	0.1450	0.1392	0.1330																																
96.2	0.1574	0.1502	0.1441	0.1380					0.1428	0.1356	0.1291	0.1231																					0.1630	0.1561	0.1620	0.1453
117.8																																				
Polystyrene Phantom																																				
9.6					0.2068	0.2025	0.1987	0.1948					0.2092	0.2048	0.2006	0.1964	0.2110	0.2066	0.2021	0.1976																
28.7					0.1973	0.1924	0.1880	0.1837					0.2004	0.1955	0.1906	0.1860	0.2026	0.1977	0.1932	0.1879																
47.9					0.1853	0.1797	0.1747	0.1698					0.1891	0.1835	0.1781	0.1731	0.1917	0.1862	0.1809	0.1755																
72.8					0.1681	0.1617	0.1560	0.1506					0.1729	0.1664	0.1605	0.1549	0.1760	0.1700	0.1640	0.1582																
97.5					0.1507	0.1437	0.1376	0.1320					0.1563	0.1491	0.1428	0.1370	0.1598	0.1532	0.1470	0.1410																
122.4					0.1336	0.1263	0.1201	0.1146					0.1397	0.1323	0.1257	0.1199	0.1437	0.1369	0.1302	0.1242																
Acrylic Plastic Phantom																																				
9.7					0.2068	0.2023	0.1985	0.1947					0.2090	0.2046	0.2005	0.1964	0.2107	0.2062	0.2020	0.1974																
29.1					0.1972	0.1921	0.1877	0.1834					0.2002	0.1951	0.1906	0.1861	0.2024	0.1973	0.1927	0.1877																
47.9					0.1854	0.1796	0.1746	0.1698					0.1890	0.1834	0.1782	0.1732	0.1917	0.1861	0.1810	0.1756																
74.8					0.1668	0.1602	0.1545	0.1490					0.1714	0.1650	0.1592	0.1535	0.1747	0.1685	0.1627	0.1569																
102.5					0.1472	0.1400	0.1339	0.1282					0.1526	0.1455	0.1394	0.1334	0.1565	0.1497	0.1435	0.1374																
128.6					0.1296	0.1221	0.1160	0.1105					0.1355	0.1282	0.1218	0.1159	0.1399	0.1327	0.1263	0.1202																
Graphite Phantom																																				
14.6	0.2049	0.1997	0.1956	0.1918	0.2070	0.2021	0.1979	0.1939	0.2086	0.2037	0.1993	0.1947																								
28.4	0.1980	0.1925	0.1878	0.1836	0.2008	0.1954	0.1908	0.1864	0.2029	0.1974	0.1927	0.1878																								
52.2	0.1827	0.1764	0.1715	0.1664	0.1868	0.1806	0.1753	0.1703	0.1891	0.1831	0.1779	0.1722																								
52.6																																				
75.0													0.1666	0.1594	0.1535	0.1480	0.1710	0.1645	0.1586	0.1532	0.1746	0.1677	0.1621	0.1561												
102.4													0.1475	0.1396	0.1332	0.1284	0.1530	0.1460	0.1396	0.1338	0.1567	0.1495	0.1432	0.1371												
103.9																																				
Polynomial Coefficients																																				
b_0																									0.2110	0.2062	0.2025	0.1989	0.2123	0.2079	0.2038	0.1998	0.2142	0.2098	0.2053	0.2012
$10^3 b_1$																									1.757	1.726	1.670	1.623	1.848	1.789	1.735	1.700	1.855	1.793	1.770	1.684
$10^6 b_2$																									1.717	0.264	-0.590	-1.878	1.697	0.758	-0.007	-1.141	2.727	1.804	0.655	0.188
$10^9 b_3$																									1.935	4.565	5.904	11.018	5.943	6.491	6.581	9.526	4.134	4.881	6.511	6.860
V, %																									0.21	0.15	0.19	0.18	0.12	0.11	0.12	0.13	0.20	0.18	0.17	0.21

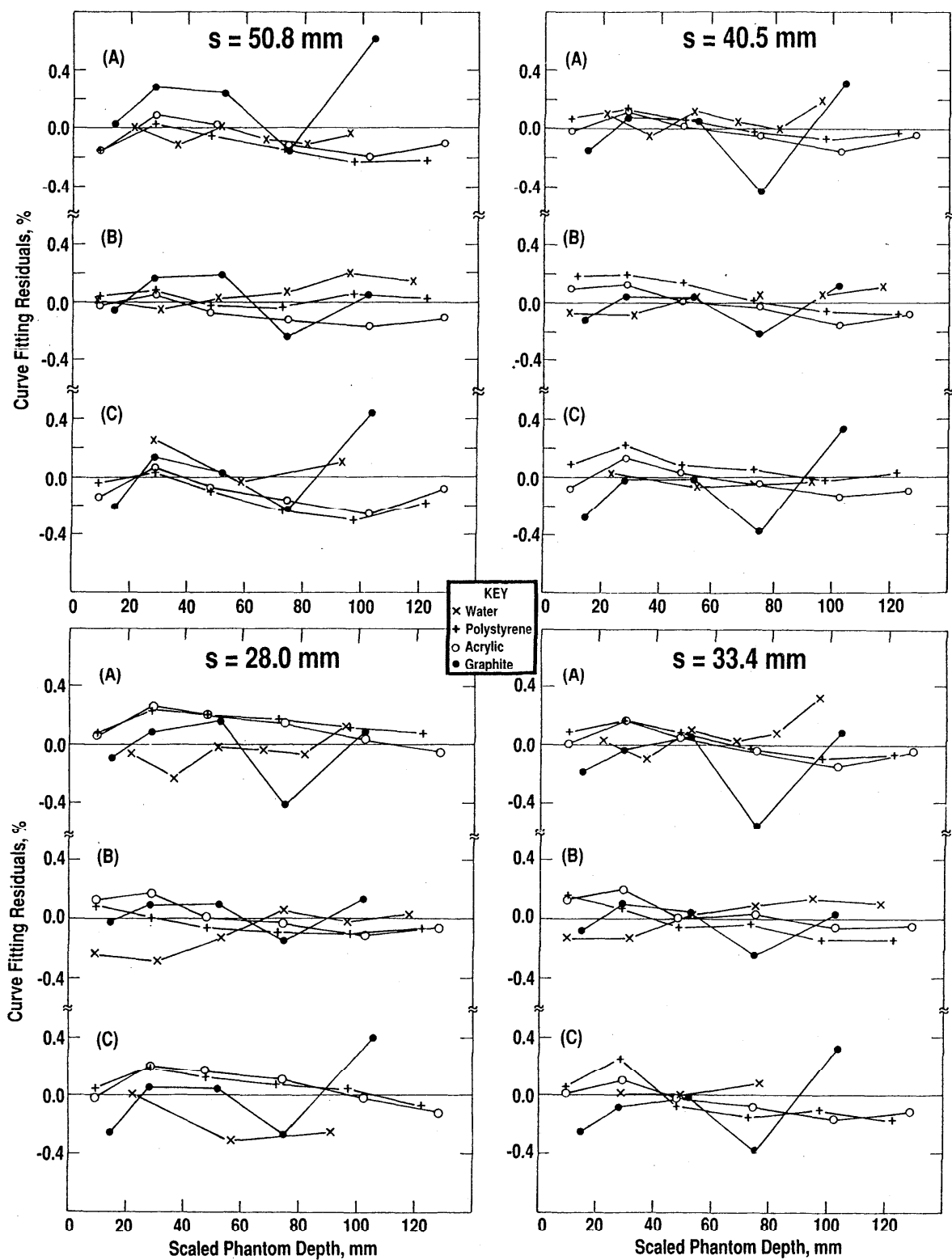


Figure 18. Residual currents in tests of fluence scaling theorem, shown as a function of collimator size and scaled phantom depth for four materials.

The only complication in this argument is that the replacement of graphite by acrylic (or polystyrene) must be done in an acrylic (or polystyrene) phantom, rather than in a water phantom. It would be expected that these changes would modify the spectra incident on the rods, but not by enough to change the numerical factors.

The replacement factor for graphite is not unity because the PL chamber graphite density (1.79 g/cm³ - reference [3]) is larger than the graphite phantom density (1.70 g/cm³ - table 12). The factor 1.001 was chosen by assuming that \bar{y} , the departure of the replacement factors from unity (0.010 for both water and polystyrene and 0.007 for acrylic) was proportional to \bar{x} , the difference between the graphite chamber mass density and the mass density of the phantom material (0.79 for water, 0.741 for polystyrene, and 0.608 for acrylic). For the graphite phantom, with a mass density difference of 0.09 g/cm³, the least squares predicted departure is $0.09(\sum \bar{x}\bar{y} / \sum \bar{x}^2) = 0.0011$.

The quantities plotted in figure 19 as a function of source distance are the total normalization factors of table 12 divided by both the PL1-11 replacement factors of table 12 and the air attenuation correction factors. These ratios have been labeled Residual Normalization Factors $F(z)$. If the prediction that photon fluence scales directly with the square of electron density were accurate, $F(z)$ would be a constant. The reasons why the Residual Normalization Factor is not constant probably include the fact that the source is not a point source. Its effective size is increased by scatter inside the head and at the collimator.

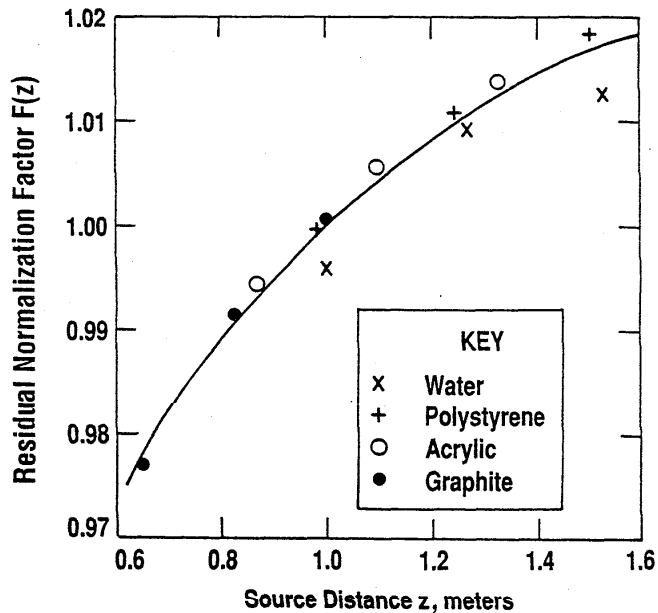


Figure 19. Residual Normalization Factors from test of fluence scaling theorem, shown as a function of source distance.

As a graphical example of the depth-current curves, figure 20 shows the three normalized curves from table 13 for collimator size 28.0 mm, along with the experimental points (or averages of the experimental points where they are too close to be separately graphed). The differences in shape are presumably caused by photon spectral changes as the source distance increases from set A to set C. These differences are not large but they are measurable. At a scaled depth of 8 mm, the ordinate for curve C is 1.4% larger than that of curve A. At a scaled depth of 128 mm, curve C is 8.9% larger than curve A. Thus spectral differences presumably account for a current difference of 7.5% over that range. For larger apertures, the difference is somewhat smaller. For $s = 50.8$ mm, the difference is only 6%.

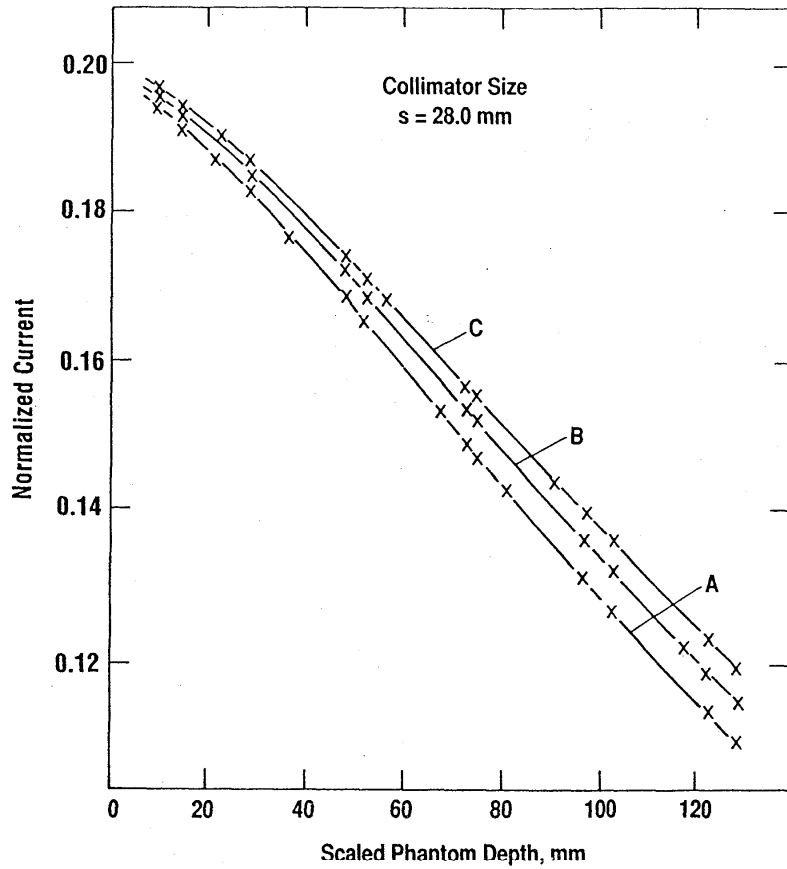


Figure 20. Normalized depth-current curves for experiments A, B, and C for collimator size 28.0 mm and several scaled phantom depths. These indicate some photon spectral change as source distances increase from A to C.

Appendix B — U.S. - U.S.S.R. Comparison

A total of six graphite transfer ionization chambers were first calibrated in a graphite phantom at NIST. Their calibrations are summarized in table 5 (for chamber PL1-11) and table 1, which shows the sensitivities relative to PL1-11 of the chambers used (PL1-14,16,17,18,19,20). The chambers were shipped to VNIIFTRI in Moscow in two sets on two different occasions, where they were also calibrated calorimetrically in a ^{60}Co beam. The first set (PL1-14,16,18) was calibrated in 1978. The second set (PL1-17,19,20) was calibrated in 1981, using a new Soviet phantom-calorimeter assembly that includes a pair of differentially connected calorimeters. The results of these comparisons are shown in table 14, using the originally reported Soviet calibrations and the more recent U.S. calibrations described in this manual.

The original intercomparison was made with preliminary calorimetric calibrations of PL1-14,16,18 using the 0.5-kCi ^{60}Co source in room B034 of NIST building 245, rather than the 10-kCi ^{60}Co source in room B036 that was used for all the calibrations described in the main body of this report. The results of that original intercomparison were described in reference [14], which listed the average Absorbed-dose (NIST)/Absorbed-dose (VNIIFTRI) = 1.022 ± 0.005 . For these B034 calibrations, the source distance was 1.00 m, the phantom depth was 5.0 g/cm², and the field size was 120 × 120 mm. These numbers differed sufficiently from the VNIIFTRI numbers (1.24-m, 3.4-g/cm², and 112-mm diameter field size) that the second intercomparison was undertaken. As shown in table 14, the average ratio Absorbed-dose (NIST)/Absorbed-dose (VNIIFTRI) = 1.0002 for the 1981 intercomparison.

In all cases, the VNIIFTRI beam was circular and the NIST beam was square in cross section, so that it was impossible to duplicate the measurement conditions from one laboratory to the other. It was decided arbitrarily that the most sensible comparison would be one in which the beam areas were identical, which accounts for the choice of NIST field sizes of 99.3 × 99.3 mm for intercomparison #1 and 101.9 × 101.9 mm for intercomparison #2.

Table 14. U.S. - U.S.S.R. intercomparisons in graphite phantoms at 20 °C and 1 atm

Intercomparison #1

A. Measurement Conditions:

Parameter	VNIIFTRI	NIST
Source distance, m	1.24	1.25
Phantom depth, g/cm ²	3.4	3.4
Field size, mm	diameter 112	99.3 × 99.3

B. Calibrations:

Chamber	VNIIFTRI (1978)	NIST (1989)	$\frac{\text{Gy(NIST)}}{\text{Gy(VNIIFTRI)}}$
PL1-14	11.30 nC/Gy	90.04 Gy/μC	1.017
PL1-16	11.35	89.80	1.019
PL1-18	10.85	93.83	1.018
		Average	1.018

Intercomparison #2

A. Measurement Conditions:

Parameter	VNIIFTRI	NIST
Source distance, m	1.00	1.00
Phantom depth, g/cm ²	4.8	4.8
Field size, mm	diameter 115	101.9 × 101.9

B. Calibrations:

Chamber	VNIIFTRI (1978)	NIST (1989)	$\frac{\text{Gy(NIST)}}{\text{Gy(VNIIFTRI)}}$
PL1-17	10.81 nC/Gy	92.44 Gy/μC	0.9993
PL1-19	10.92	91.70	1.0014
PL1-20	11.03	90.65	0.9999
		Average	1.0002

Appendix C — U.S. - Canada Comparison

Two graphite transfer ionization chambers were first calibrated in a water phantom at NIST. Their calibrations are summarized in eq (21), for chamber PL1-11, and table 1, which shows the sensitivities relative to PL1-11 of the two chambers (PL1-17,19). The chambers were shipped to the National Research Council (NRC) in Ottawa, where they were also calibrated calorimetrically in a ^{60}Co beam. The results of this intercomparison is shown in table 15, using the originally reported Canadian calibrations and the more recent U.S. calibrations described in this manual. On the average, the ratio Absorbed-dose (NIST)/Absorbed-dose (NRC) = 1.0045. Based on the original U.S. calibrations, this ratio was reported in reference [14] as 1.003 ± 0.002 .

Table 15. U.S. — Canada (National Research Council) intercomparisons in water phantoms at 0 °C and 1 atm (101.325 kPa)

A. Measurement Conditions:

Parameter	NRC	NIST
Source distance, m	1.0	1.0
Phantom depth, mm	50	50
Field size, mm	100 × 100	100 × 100

B. Calibrations

Chamber	NRC (1978)	NIST (1989)	$\frac{\text{Gy(NIST)}}{\text{Gy(NRC)}}$
PL1-17	96.0 Gy/ μC	96.21 Gy/ μC	1.0022
PL1-19	94.8	95.44	1.0068
			Average
			1.0045

Appendix D — U.S. - Sweden Comparison

Two liquid ionization chambers were transported from Sweden, where they had been calibrated in terms of absorbed-dose to water in a ^{60}Co beam by three methods: air-ionization-chamber dosimetry, water calorimetry, and ferrous-sulphate dosimetry. The internal agreement between these three methods was of the order of 0.4%. These two chambers were then calibrated in the NIST ^{60}Co beam at several depths in the water phantom. The NIST calibration data are shown in table 16A, and the NIST and Swedish calibrations are compared in table 16B, where the Swedish numbers came from ferrous-sulfate dosimetry.

The NIST calibrations in table 16 differ from the numbers recently published in reference [15], for several reasons, most of which are mentioned in sections 5, 6.2, and 6.3. The agreement between the NIST and Swedish calibrations is not nearly as good as the published values (0.02% for chamber #1 and 0.19% for chamber #2), but is still within the overall uncertainty of the NIST calibration alone, without considering uncertainties in the Swedish calibrations.

Table 16. Calibration of Swedish liquid ionization chambers in a water phantom

A NIST measurements as a function of depth in water, using the 50.8 mm collimator jig.

Chamber number	Source distance m	Water depth mm	Absorbed dose-rate mGy/s	Measured current nA	Chamber calibration Gy/ μC	Average Gy/ μC
1	1.0000	33.8	12.247	0.19252	63.61	63.68
		51.9	11.499	0.18056	63.69	
		52.4	11.478	0.18037	63.64	
		53.2	11.443	0.17984	63.63	
		73.1	10.566	0.16598	63.66	
		93.6	9.653	0.15150	63.72	
		113.1	8.804	0.13819	63.71	
		131.4	8.040	0.12614	63.74	
2	1.0005	51.3	11.513	0.17960	64.11	64.14
		73.4	10.542	0.16432	64.16	

B U.S. — Swedish intercomparison

Chamber number	Sweden (1982) Gy/ μC	NIST (1989) Gy/ μC	$\frac{\text{Gy(NIST)}}{\text{Gy(Sweden)}}$
1	63.23	63.68	1.0071
2	63.82	64.14	1.0050

Appendix E - Sample Calibration Report

DG 8787/87
DB 843/42
TFN 240907
1987 Dec 23

Page 1 of 4

U. S. DEPARTMENT OF COMMERCE
NATIONAL BUREAU OF STANDARDS
GAITHERSBURG, MD 20899

REPORT OF TEST

Parallel plate ionization chamber, mounted in a polystyrene plate

Model MPPK, Serial Number 278

Manufactured by Memorial Hospital
New York, NY 10021

Submitted by _____

Received at NBS 1987 Oct 21
Calibration date 1987 Dec 4

The calibration factors given in this report are quotients of the absorbed-dose rate to water, measured in a polystyrene phantom irradiated with cobalt-60 gamma rays, divided by the ionization chamber current generated by that radiation. The average ion current used to compute the calibration factor is based on currents measured with the outer electrode of the triax connector at the stated polarity and potential. The middle electrode was grounded and the central pin was connected to the electrometer input. The currents were normalized to one standard atmosphere and 22 degrees Celsius. Use of the chamber at other pressures and temperatures requires correction of the ion currents to these reference conditions. The correction factor F is computed from the following expression:

$$F = (273.15 + T)/(295.15 H)$$

where T is the temperature in degrees Celsius, and
H is the pressure expressed as a fraction of a standard atmosphere.
(1 standard atmosphere = 101.325 kilopascals = 1013.25 millibars = 760 mmHg).

The absorbed-dose rate to water at the calibration position in polystyrene was determined as described on page 4. The calibration factors given on page 3 apply only for the conditions given in the table, but the factors vary slowly with depth in the phantom and with field width, and are nearly independent of source-chamber distance.

The chamber was received with no information about the chamber inner dimensions. These were assumed to be the same as the dimensions of the Memorial Hospital chamber described in J. G. Holt, et al., "Absorbed dose measurements using parallel plate polystyrene phantoms," Int. J. Rad. Oncol. Biol. Phys. 2, 2031-2038 (1979).

Calibration factors are given at two depths. At the smaller depth, no other plate was placed on top of the chamber block. At the larger depth, an additional 25-cm square, 6-mm-thick polystyrene plate was added. In both cases, the chamber mount was backed by a 30-cm-diameter, 12-cm-thick polystyrene block.

The uncertainty of the absorbed dose measurements is under investigation. It is expected to be not greater than 2% at the 95% confidence level; the accuracy of the current measurements is believed to be within a few tenths of a percent.

Information on technical aspects of this report may be obtained from J. S. Pruitt, Radiation Physics C214, National Bureau of Standards, Gaithersburg, MD 20899, (301) 975-5587.

Calibration performed by J. S. Pruitt *JSP*

Report approved by R. Loevinger *RL*

For the Director
by

Randall S. Caswell

Randall S. Caswell, Chief
Ionizing Radiation Division
Center for Radiation Research
National Measurement Laboratory


NATIONAL BUREAU OF STANDARDS REPORT OF CALIBRATION

Parallel Plate Chamber
Model MPPK Serial Number 278
Collection potential: -300 V
Not tested for atmospheric connection

1	2	3	4	5	6
Beam Code	Calibration Factor 22 deg C and 1 atm (Gy/nC)	Polystyrene Depth (mm)	Source Distance (m)	Beam Width (mm)	Dose Rate (mGy/s)
60Co	0.0334 0.0333	4 10	0.984	94	7

During calibration, the cavity was positioned in the center of the beam with the polystyrene plate perpendicular to the beam direction. The chamber surface nearest the source of radiation had a small air vent hole. A reference plane was defined, which is believed to coincide with the inside surface of the electrode nearest the source of radiation. This reference plane is parallel to the surface of the polystyrene plate, at a depth of 4 mm.

2E-15 A was the average leakage current measured during the calibration.

Checked by 

EXPLANATION OF COLUMNS IN THE CHAMBER CALIBRATION TABLE

1. The beam code identifies the radiation source used for the calibration.
2. The calibration factor defined in the body of the report, in SI units (grays per nanocoulomb). Use of the calibration factor to determine absorbed dose to water is discussed on page 4.
3. The depth from the phantom surface to the reference plane.
4. The distance between the radiation source and the reference plane.
5. The beam width in the reference plane measured in air between the 50-percent intensity lines. The cross-section of the beam was square.
6. The absorbed-dose rate at which the calibration was performed. If the chamber is used to measure an absorbed-dose rate that is significantly different from that used for the calibration it may be necessary to correct for ion recombination. The stated calibration factor has not been corrected for ion recombination.

The NBS cobalt-60 beam had previously been calibrated in absorbed dose to water at a source distance of 1 meter as described in: J. S. Pruitt, S. R. Domen, and R. Loevinger, "The graphite calorimeter as a standard of absorbed dose for cobalt-60 gamma radiation," J. Res. Nat. Bur. Stand. 86, 495-502 (1981). Figure 3 of this article illustrates the dependence of an ionization chamber calibration on phantom depth, field size, and source distance. The calibration factors listed in column 2 of the table were obtained from this water calibration using current measurements in a polystyrene phantom, with the chamber reference plane at a source distance of 0.984 meters, to insure a spectral distribution the same as at 1 meter in water, as described in: J. S. Pruitt and R. Loevinger, "The photon-fluence scaling theorem for Compton-scattered radiation," Med. Phys. 9, 176-179 (1982). The dose rate in a water phantom at source distance d in a cobalt-60 beam may be obtained from measurements of current in a polystyrene phantom at source distance $0.984 d$, and is:

$$D_{\text{water}} = (0.984)^2 \times I(0.984d) \times N \text{ Gy/s}$$

where $I(0.984d)$ is the normalized current (in nA) in the polystyrene phantom at $0.984 d$, and N is the calibration factor (in Gy/nC) from column 2. The water depths to which these calibrations apply are the polystyrene depths listed in column 3 of the table, divided by 0.984.

REFERENCES

- [1] Pruitt, J. S., Domen, S. R., and Loevinger, R., "The Graphite Calorimeter as a Standard of Absorbed Dose for Cobalt-60 Gamma Radiation," J. Res. Natl. Bur. Stand. (U.S.) 86, 495 (1981).
- [2] Domen, S. R. and Lamperti, P. J., "A Heat-Loss-Compensated Calorimeter: Theory, Design, and Performance," J. Res. Natl. Bur. Stand. (U.S.) 78A, 595 (1974).
- [3] Pruitt, J. S. and Loevinger, R., "Ionization Chamber for Absorbed-Dose Calibration," Proceedings of Symposium on Measurements for the Safe Use of Radiation; 1976 March 1-4; Gaithersburg, MD, National Bureau of Standards (U.S.) Spec. Publ. 456: 37-39, 1976 November.
- [4] NCRP Report No. 58, "A Handbook of Radioactivity Measurements and Procedures (Second Edition)," National Council on Radiation Protection and Measurements, Bethesda, MD, 20814 (1985), table 9.
- [5] Domen, S. R., private communication.
- [6] Quinn, T. J., "Report of the Director, Bureau Internationale des Poids et Mesures (BIPM)," 1987 October-1988 September, Sevres, France.
- [7] Loevinger, R., "A Formalism for Calculation of Absorbed-Dose to a Medium from Photon and Electron Beams," Med. Phys. 8, 1 (1981).
- [8] Burlin, T. E., "Cavity-Chamber Theory," Chapter 8, Radiation Dosimetry, Vol. 1, Fundamentals; Second Edition: edited by F. H. Attix, W. C. Roesch, and E. Tochilin. Academic Press (1968).
- [9] Pruitt, J. S. and Loevinger, R., "The Photon-Fluence Scaling Theorem for Compton Scattered Radiation," Med. Phys. 9, 176 (1982).
- [10] Hubbell, J. H., "Photon Mass Attenuation and Mass Energy-Absorption Coefficients for H, C, N, O, Ar and Seven Mixtures from 0.1 keV to 20 MeV," Radiat. Res. 70, 58 (1977).
- [11] Bruce, W. R. and Johns, H. E., "The Spectra of X-Rays Scattered in Low Atomic Number Materials," Brit. J. Radiol. Supplement No. 9, British Institute of Radiology, London (1960).
- [12] Seltzer, S. M., Hubbell, J. H., and Berger, M. J., "Some Theoretical Aspects of Electron and Photon Dosimetry," Proceedings of IAEA International Symposium on National and International Standardization of Radiation Dosimetry, 5-9 December 1977, Atlanta, GA; IAEA-SM-222/05; International Atomic Energy Agency, Vienna (1978).
- [13] Colle, R. Private communication concerning a meeting of a Working Group on the Statement of Uncertainties, Bureau Internationale des Poids et Mesures, Sevres, France, October 1980.
- [14] Proceedings of the 5th Meeting of Section I of the Comité Consultatif pour les Étalons de Mesure des Rayonnements Ionisants (CCEMRI), 28-30 May 1979, at the Bureau International des Poids et Mesures, Sevres, France.
- [15] Mattsson, O., Svensson, H., Wickman, G., Domen, S. R., Pruitt, J. S., and Loevinger, R., "Absorbed Dose to Water: Comparison of Several Methods Using a Liquid Ionization Chamber," submitted for publication in Acta Radiologica Oncology.

U.S. DEPT. OF COMM. BIBLIOGRAPHIC DATA SHEET <i>(See instructions)</i>	1. PUBLICATION OR REPORT NO. NIST/SP-250/40	2. Performing Organ. Report No.	3. Publication Date October 1990
4. TITLE AND SUBTITLE ABSORBED-DOSE CALIBRATION OF IONIZATION CHAMBERS IN A ⁶⁰ Co GAMMA-RAY BEAM			
5. AUTHOR(S) John S. Pruitt			
6. PERFORMING ORGANIZATION <i>(If joint or other than NBS, see instructions)</i> NATIONAL INSTITUTE OF STANDARDS AND TECHNOLOGY <i>(formerly NATIONAL BUREAU OF STANDARDS)</i> U.S. DEPARTMENT OF COMMERCE GAITHERSBURG, MD 20899		7. Contract/Grant No.	8. Type of Report & Period Covered Final
9. SPONSORING ORGANIZATION NAME AND COMPLETE ADDRESS <i>(Street, City, State, ZIP)</i> Same as item #6			
10. SUPPLEMENTARY NOTES <input type="checkbox"/> Document describes a computer program; SF-185, FIPS Software Summary, is attached.			
11. ABSTRACT <i>(A 200-word or less factual summary of most significant information. If document includes a significant bibliography or literature survey, mention it here)</i> Measurement Service C.1 from National Institute of Standards and Technology (NIST) publication SP 250 provides calibrations for customer-owned ionization chambers so that they may be used to determine absorbed dose to water in ⁶⁰ Co gamma-ray beams. The calibrations are based on calorimetric measurement of absorbed dose to graphite in a graphite phantom. Transformation of the calibrations to a water phantom is made with a specially-designed graphite ionization chamber, and requires knowledge of photon mass attenuation coefficients and the perturbation of the graphite chamber in the water medium. The determination of these quantities is described in detail, along with the operational techniques normally used to transfer the calibration to customer-owned chambers. Appendix A lists experimental data used to test the photon-fluence scaling theorem. Appendices B, C, and D describe international comparisons of the chamber calibrations, and Appendix E shows a sample calibration report.			
12. KEY WORDS <i>(Six to twelve entries; alphabetical order; capitalize only proper names; and separate key words by semicolons)</i> absorbed dose; calibration; calorimeter; cobalt-60; ionization chamber; photon fluence			
13. AVAILABILITY <input checked="" type="checkbox"/> Unlimited <input type="checkbox"/> For Official Distribution. Do Not Release to NTIS <input checked="" type="checkbox"/> Order From Superintendent of Documents, U.S. Government Printing Office, Washington, D.C. 20402. <input checked="" type="checkbox"/> Order From National Technical Information Service (NTIS), Springfield, VA. 22161			14. NO. OF PRINTED PAGES 54
			15. Price

THE SP 250 SERIES ON NIST MEASUREMENT SERVICES*

SP 250-1	Spectral Radiance Calibrations PB87179883	SP 250-19	Calibration of Gamma-Ray-Emitting Brachytherapy Sources PB89193858
SP 250-2	Far Ultraviolet Detector Standards PB87227609	SP 250-20	Spectral Irradiance Calibrations PB88123781
SP 250-3	Radiometric Standards in the Vacuum Ultraviolet PB87227625	SP 250-21	Calibration of Beta-Particle Radiation Instrumentation PB88201579
SP 250-4	Fricke Dosimetry in High-Energy Electron Beams PB88110374	SP 250-22	Platinum Resistance Thermometer Calibrations PB88138367
SP 250-5	Alpha-Particle Calibrations PB88168620	SP 250-23	Liquid-in-Glass Thermometer Calibration Service PB89128888
SP 250-6	Regular Spectral Transmittance PB88108550	SP 250-24	Standard Cell Calibrations PB88123690
SP 250-7	Radiance Temperature Calibrations PB88123674	SP 250-25	Calibration Service for Inductive Voltage Dividers
SP 250-8	Spectral Reflectance PB88109905	SP 250-26	NBS Phase Angle Calibration Services PB88225636
SP 250-9	Calibration of Beta-Particle-Emitting Ophthalmic Applicators PB88108535	SP 250-27	AC-DC Difference Calibrations PB892222616
SP 250-10	Radioactivity Calibrations with the "4 π " Gamma Ionization Chamber and Other Radioactivity Calibration Capabilities PB88123708	SP 250-28	Solid-State DC Voltage Standard Calibrations PB88168703
SP 250-11	Dosimetry for High Dose Applications PB88201587	SP 250-29	Traceable Frequency Calibrations PB88168364
SP 250-12	Neutron Personnel Dosimetry PB87227617	SP 250-30	GOES Satellite Time Code Dissemination: Description and Operation PB88168760
SP 250-13	Activation Foil Irradiation with Californium Fission Sources PB88217443	SP 250-31	Mass Calibrations PB89153894
SP 250-14	Activation Foil Irradiation by Reactor Cavity Fission Sources PB88217435	SP 250-32	A Calibration Service for 30 MHz Attenuation and Phase Shift PB88238324
SP 250-15	Photometric Calibrations PB88153747	SP 250-33	A Calibration Service for Voltage Transformers and High-Voltage Capacitors PB882252903
SP 250-16	Calibration of X-Ray and Gamma-Ray Measuring Instruments PB88211826	SP 250-34	High Vacuum Standard and Its Use PB89193841
SP 250-17	The NBS Photodetector Spectral Response Calibration Transfer Program PB88201595	SP 250-35	The Calibration of Thermocouples and Thermocouple Materials PB89209340
SP 250-18	Neutron Source Strength Calibrations PB88211818	SP 250-40	Absorbed-Dose Calibration of Ionization Chambers in a ⁶⁰ Co Gamma-Ray Beam

* Entries containing a stock number (SN003-003-) and price can be purchased from the Superintendent of Documents, U.S. Government Printing Office, Washington, DC 20402. GPO will accept checks, money orders, VISA, and MasterCard. For more information, or to place an order, call (202) 783-3238. Be sure to cite the stock number on all orders.

Entries containing PB numbers can be purchased from the National Technical Information Service, Springfield, VA 22161. NTIS will accept American Express in addition to the payment methods listed for GPO. For more information call (703) 487-4650; to place an order call (800) 336-4700. Be sure to cite the PB number on all orders.

Entries without stock or PB numbers are in preparation.

U.S. Department of Commerce
National Institute of Standards and Technology
(formerly National Bureau of Standards)
Gaithersburg, MD 20899

Official Business
Penalty for Private Use \$300